

2 **Emerging technologies in the field of thermometry**

3 **S Dedyulin<sup>1</sup>, Z Ahmed<sup>2</sup> and G Machin<sup>3</sup>**

4 <sup>1</sup>Metrology Research Centre, National Research Council of Canada, Canada

5 <sup>2</sup>Physical Measurement Laboratory, Sensor Science Division, National Institute of  
6 Standards and Technology, USA

7 <sup>3</sup> Temperature Standards, National Physical Laboratory, UK

8 E-mail: zeeshan.ahmed@nist.gov

9 **Abstract.**

10 The past decade saw the emergence of new temperature sensors that have the  
11 potential to disrupt a century-old measurement infrastructure based on resistance  
12 thermometry. In this review we present an overview of emerging technologies that  
13 are either in the earliest stages of metrological assessment or in the earliest stages of  
14 commercial development and thus merit further consideration by the measurement  
15 community. The following emerging technologies are reviewed: Johnson noise  
16 thermometry, optical refractive-index gas thermometry, Doppler line broadening  
17 thermometry, optomechanical thermometry, fiber-coupled phosphor thermometry,  
18 fiber-optic thermometry based on Rayleigh, Brillouin and Raman scattering, fiber-  
19 Bragg-grating thermometry, Bragg-waveguide-grating thermometry, ring-resonator  
20 thermometry, and photonic-crystal-cavity thermometry. For each emerging technology,  
21 we explain the working principle, highlight the best known performance, list advantages  
22 and drawbacks of the new temperature sensor and present possibilities for future  
23 developments.

24 *Keywords:* emerging technology, temperature sensor, photonic thermometry

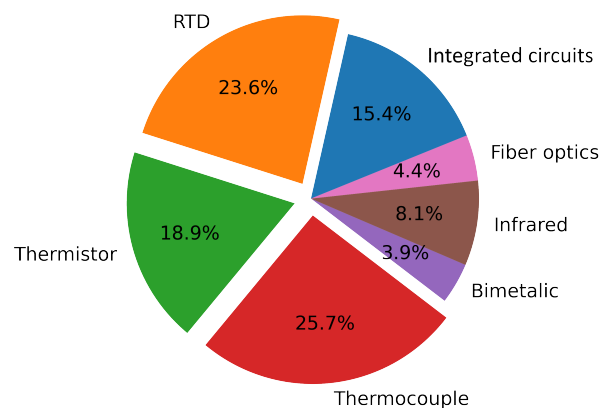


**Figure 1.** Percentage market share for different temperature sensors in 2017 (total market size: 6.3 billion USD) [1].

## 1. Introduction

Temperature measurements play a central role in every aspect of modern life, from advanced manufacturing to home cooking. Consequently, the global temperature-sensor market is a multi-billion dollar enterprise that is expected to grow to over nine billion US dollars by the year 2026, as the use of temperature sensors continues to proliferate [1]. There exists a variety of temperature sensors that use different physical principles to measure temperature and vary greatly in their accuracy, cost, size, level of training required, etc. The three most common types of temperature sensors (see figure 1), ranging in accuracy from high to low are: Resistance Temperature Detector (RTD), Negative Temperature Coefficient (NTC) thermistor, and thermocouple. Each of these three types of sensors measures the change in the electrical quantities — resistance and/or voltage — with temperature and each one of them has a measurement history going back for more than hundred years. Over this time period, the design of these sensors has been continuously improved to meet most users' measurement needs, making it easier to overlook their remaining drawbacks while focusing on their numerous advantages instead [2–4]. For example, platinum (wire) resistance thermometers (PRTs) — an RTD type sensor — when deployed in specialized temperature calibration laboratories, can measure temperature with uncertainties approaching a few hundreds of  $\mu\text{K}$  over the span of 1000 K [5]. However, these are known to be sensitive to mechanical shock and thermal stress, are prone to chemical contamination, and suffer from ionizing radiation damage and electromagnetic interference (EMI) which limits their performance outside of temperature calibration laboratories [2].

The inevitable drawbacks of the existing temperature sensors and the specific requirements for emerging applications of temperature sensors are powerful motivations for developing novel technologies targeted towards meeting present and future needs of the community. The past few years have seen the emergence of new temperature sensors, based on different physical principles such as: photonics, quantum optomechanics, noise

1 thermometry, etc. Motivations behind the development of these emerging technologies  
 2 are multi-faceted, ranging from the desire for low-cost, small, *in-situ* temperature  
 3 sensors for critical infrastructure monitoring applications (e.g. fiber-optic thermometry),  
 4 to embedded sensors for quantum computing and quantum information systems (e.g.  
 5 photonic and quantum optomechanical thermometry), to the development of portable  
 6 thermodynamic temperature sensors (e.g. optical refraction, Doppler broadening and  
 7 quantum optomechanical thermometry). Leveraging the vast economies of scale provided  
 8 by the telecommunications industry’s infrastructure and metrology expertise developed  
 9 for frequency metrology, these techniques hold the promise of enabling fit-for-purpose,  
 10 cost-effective measurement solutions that may ultimately meet or out-perform legacy  
 11 devices. In particular, the development of ultra-stable photonic thermometers that show  
 12 minimal drift over decadal time spans or thermodynamic temperature sensors, based  
 13 on quantum properties of matter, could dramatically disrupt the calibration-centered  
 14 metrology ecosystem.

15 In this review paper we focus on the emerging technologies for measuring temperature  
 16 that are either in the earliest stages of metrological assessment (e.g. fiber-optic  
 17 thermometry) or in the earliest stages of commercial development (e.g. Johnson noise  
 18 thermometry) and thus merit further consideration by the community (see figure 2). The  
 19 most common performance metrics/requirements to consider at this stage are described  
 20 in section 2 with specific examples from emerging technologies. The details of these  
 21 technologies are then described in separate sections, devoted to primary thermometry  
 22 (section 3) and approximations of defined scales (section 4). Note that we have adhered  
 23 to the classification suggested in the *Mise en pratique* for the definition of the kelvin in  
 24 the SI [6], where the distinction is made between:

- 25 – *Primary thermometry* (e.g. acoustic gas thermometry (AGT [7]) and Johnson noise  
 26 thermometry (JNT [8])), which is carried out using a thermometer, based upon a  
 27 well-understood physical system, for which the equation of state, describing the  
 28 relation between thermodynamic temperature  $T$  and other independent quantities,  
 29 such as the ideal gas law or Planck’s equation, can be expressed explicitly without  
 30 unknown or significantly temperature-dependent constants. It can be absolute or  
 31 relative primary thermometry.
- 32 – *Defined temperature scales* (e.g. International Temperature Scale of 1990 (ITS-  
 33 90) [9, 10]), which assign temperature values, determined by primary thermometry,  
 34 to a series of naturally occurring and highly reproducible states (e.g., the freezing  
 35 and triple points of pure substances). Defined scale also covers a specification of the  
 36 interpolating or extrapolating instruments for a particular sub-range of temperature  
 37 and define necessary interpolating or extrapolating equations.
- 38 – *Approximations of defined scales* (e.g. approximations of ITS-90 [4]), where fixed  
 39 points, interpolating or extrapolating instruments, and interpolating or extrapolating  
 40 equations are different from those specified in the defined scales, but any differences  
 41 from a scale are sufficiently well-understood.

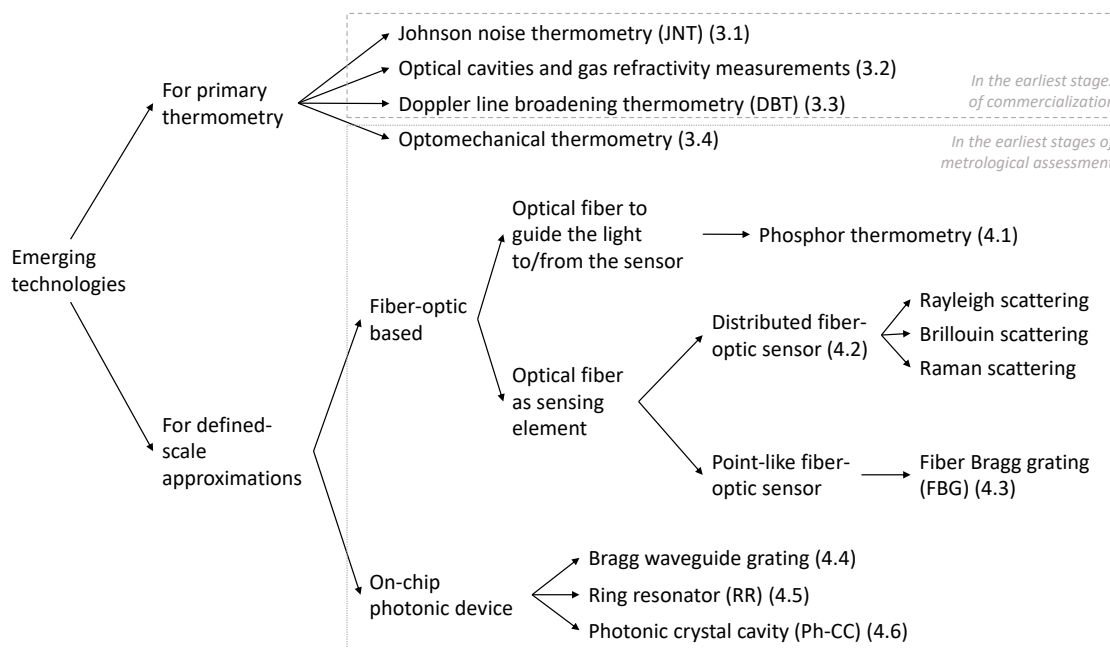


**Figure 2.** Schematic outline of the emerging technologies covered in this review with the individual section numbers, identified in the brackets. The selection criteria for this review are also shown in light gray.

1 For each emerging technology, we provide the following: a short description, the best  
 2 known performance, advantages, drawbacks and summaries of the current work to  
 3 overcome these drawbacks. The intercomparison of the emerging technologies and the  
 4 future outlook are presented in section 5. Given the size of the surveyed field, the amount  
 5 of information required, and the rapidly evolving nature of the field, the list of the  
 6 emerging technologies described below is not exhaustive and the performance metrics  
 7 provided are best available estimates that will continue to evolve.

## 8 2. Performance metrics for selecting an emerging temperature sensor

9 Similarly to a typical technology life cycle [11], one can distinguish the following stages  
 10 in the development of a new (temperature) sensor:

- 11 – *Research and development stage*, when a new temperature sensor is proposed and  
 12 temperature sensitivity is experimentally verified (typically performed in a research  
 13 laboratory and results reported in academic journals). The questions typically asked  
 14 by a researcher at this point are: “Can this sensor measure temperature?” and  
 15 ”What are its advantages as compared to the existing technologies?”.
- 16 – *Ascent stage*, when the claims from the previous stage are carefully assessed (typically  
 17 performed in a calibration laboratory; the results of the testing are usually in the  
 18 form of internal reports, not available to the general public). At this stage, the  
 19 objective answers are provided to the questions: “What is the accuracy of the

1 sensor?”, “Does it conform to the specifications proposed at the research stage?” and  
2 “Can I trust it?”. This stage will determine whether or not the sensor’s development  
3 will move to the next stage and the range of potential applications.

- 4 – *Stage of maturity*, when the sensor is mass produced and accepted by the  
5 measurement community. Hereafter, only relatively small incremental improvements  
6 to the sensor’s design will be made and their own implementation will again follow  
7 the three stages of the development cycle above.

8 As mentioned previously in the introduction, this review paper is primarily concerned  
9 with temperature sensors that are currently either under metrological assessment or at  
10 the beginning of commercial development and thus belong to the ascent stage described  
11 above. At this stage, a few sensor characteristics deserve particular considerations [12]  
12 as described further below.

- 13 • *Relationship* between temperature and the physical property that changes with  
14 temperature (thermometric property) should be well-established. For primary  
15 thermometers this relationship is based on well-understood physical principles and  
16 has an exact functional form, while for the rest it is often established empirically  
17 and has multiple fitting parameters. The fitting requires multiple measurements  
18 of the same sensor over a range of temperatures — to determine the functional  
19 form of the relationship, its repeatability and hysteresis — and, ideally, additional  
20 multiple measurements of the different sensors of the same type — to establish the  
21 reproducibility of the relationship. For example, as we describe in detail in section  
22 4.3, the response of a Fiber-Bragg-Grating (FBG) thermometers to temperature  
23 changes consists of two parts: 1) Thermal expansion of the optical fiber and 2)  
24 Changes in the refractive index due to the thermo-optic effect (TOE). Yet, most  
25 research papers model the thermal response as: a) Arising due to the TOE alone —  
26 since the thermo-optic coefficient (TOC) of silica is a factor of ten larger than the  
27 thermal expansion — and b) A linear relationship — thus assuming that silica’s TOC  
28 does not change with temperature. However, careful examination [13] reveals that  
29 to achieve smaller uncertainties a quadratic thermal response needs to be considered.  
30 Another example is the tacit assumption that high-temperature fiber Bragg gratings  
31 are identical when produced with great care under as identical conditions as possible  
32 (see e.g. [14, 15]). Yet, this might well not be the case as illustrated in figure 3 using  
33 the results obtained with unpackaged  $\pi$ -phase-shifted Type II FBGs [16] at 1000 °C,  
34 produced under identical laser-writing conditions [17]. Note how the gratings 1 and  
35 5, produced under identical conditions from the same batch of fiber, identically  
36 treated and measured in the same furnace under identical conditions, nevertheless  
37 manifest an opposite drift behaviour at 1000 °C. In other words, reproducibility of  
38 this particular FBG thermometer is rather poor.
- 39 • *Accuracy* in the context of present discussion is defined as the degree of conformity  
40 of an indicated value to a recognized standard value, or ideal value [18]. Accuracy  
41 will usually be expressed as the uncertainty in the measurement. Estimating the

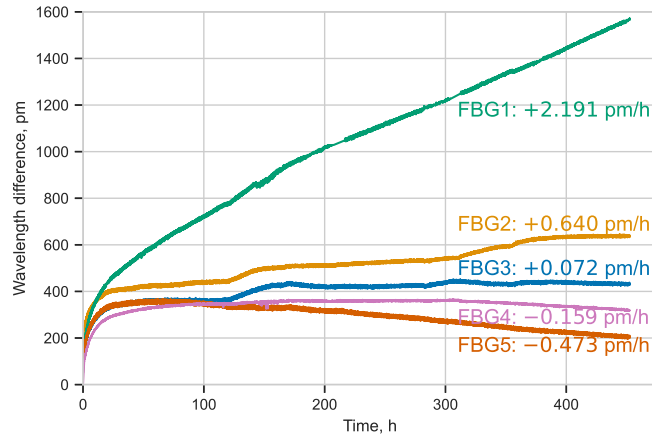


**Figure 3.** Five unpackaged  $\pi$ -phase-shifted Type II FBGs at 1000 °C, produced and treated identically, exhibit different drift behaviour in terms of both magnitude and sign (reproduced from [17]).

1 uncertainty in a measurement can be difficult, as it depends on a large number of  
 2 of (often unknown in advance) factors, such as the construction of the sensor, the  
 3 temperature range, the environment the sensor is exposed to, and how it is used. In  
 4 addition, the uncertainties can alter over the lifetime of an individual sensor. Full  
 5 accuracy (uncertainty) assessment is rarely done in the research and development  
 6 stage, and thus assessing the typical accuracy of the emerging technology becomes  
 7 the task of the calibration laboratory in the ascent stage. It is typically done in terms  
 8 of uncertainty budget; recent examples for photonic thermometry can be found  
 9 in [13,19,23]. In that specific example, it was found that the measurement uncertainty  
 10 in photonic thermometry is dominated by limitations of the wavelength measurement  
 11 scheme [13], long-term drift/hysteresis in the device and packaging [13, 19–21], self-  
 12 heating [22], wavelength uncertainty within the spectral scan [23] and fabrication  
 13 imperfections [20]. The measurement scheme, either via a wavelength-swept method  
 14 or laser locking, limits the accuracy with which a peak center can be determined.  
 15 Effects such as self-heating depend on properties of the material (bandgap and  
 16 heat capacity), operating wavelength, optical quality factor of the device itself  
 17 and input laser power. The impact of fabrication imperfections, ghost resonances  
 18 from reflections of photonic inter-connects, modal dispersion and mode-mixing in  
 19 multimode waveguides need to be better understood.

- 20 • *Resolution*, or the smallest change that can be detected in the measured quantity  
 21 above the measurement noise, is typically a function of both the sensor design and  
 22 the measurement parameters/scheme. For example, in the case of photonics-based  
 23 thermometry, the two sensor characteristics that determine the resolution limit for  
 24 steady-state and time-limited temperature measurements are: the quality factor  
 25 and the integration time, with the former being determined by the sensor’s design,  
 26 while the latter is, to a large extent, a property of the measurement scheme. The

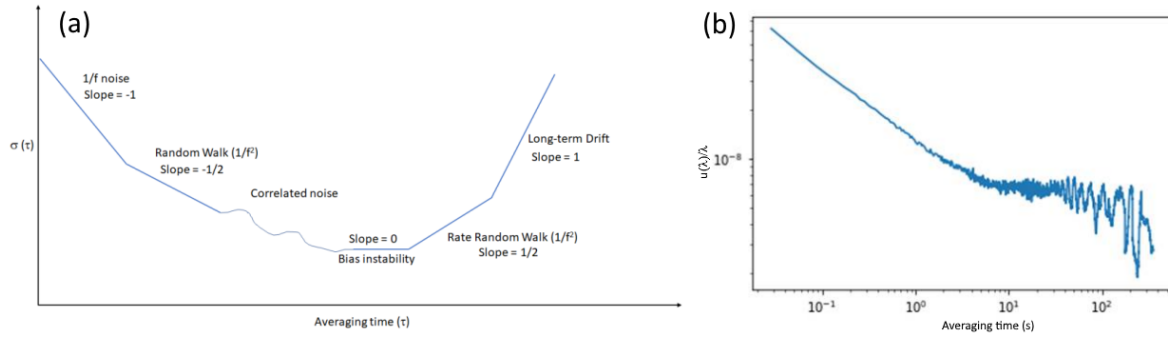


**Figure 4.** (a) A theoretical Allan deviation plot with the noise sources identified. (b) An example of the Allan deviation plot for a  $\pi$ -phase-shifted FBG inside the ice point.

quality factor (Q-factor) is defined as  $Q = \lambda_m/\text{FWHM}$ , where FWHM refers to the resonance bandwidth, measured at the full width at half-maximum and  $\lambda_m$  is the resonance wavelength. From a practical point-of-view the quality factor describes how narrow a resonance feature is, how accurately the resonance peak center can be determined, and as such effectively sets the limit on the resolution that is achievable with that device. In silicon resonators Q-factors of over 400,000 have been reported [24, 25] though a Q of 100,000 should be sufficient for a sub-mK temperature resolution [26]. Nonlinear effects [27, 28] such as two-photon absorption and Kerr effect grow in prominence with increasing Q-factor, which can lead to observation of confounding effects such as self-heating and optical bi-stability [28, 29]. These effects, if not accounted for and/or minimized can have a considerable effect on the achievable uncertainty of a photonic thermometer [26]. The integration time, or the time span over which the thermometer signal is averaged, can significantly impact the measurement's noise floor. The integration time-limited uncertainty in photonics-based thermometry is most often reported as an Allan deviation plot [30] that allows one to distinguish between different noise sources (see figure 4). It is desirable for photonic thermometers to show a noise floor of at most  $1 \mu\text{K}$  to  $1 \text{ mK}$  over integration times of  $1000 \text{ s}$  to  $1 \text{ ms}$ , respectively. We note that fundamentally the resolution limit in photonic “whispering gallery” mode resonators is primarily set by the thermo-refractive noise, which sets the relative frequency stability limit at around one part per  $10^{-12}$  per  $1 \text{ s}$  integration time [31, 32]. Other sources of noise include thermo-elastic, thermodynamic, photothermal, pondermotive and self-modulation noise [31, 32].

- *Stability* of the sensor with respect to time can be conventionally divided into two parts: short-term (usually on the scale of hours to several days) and long-term (usually on the scale of weeks to decades). The presence of long-term stability typically implies the presence of short-term stability but not vice versa. Short-term stability is typically measured as part of assessing the accuracy claim above and contributes to the uncertainty budget of the temperature sensor. It is impractical, however, to hold a thermometer for ten years just to prove that it has a certain

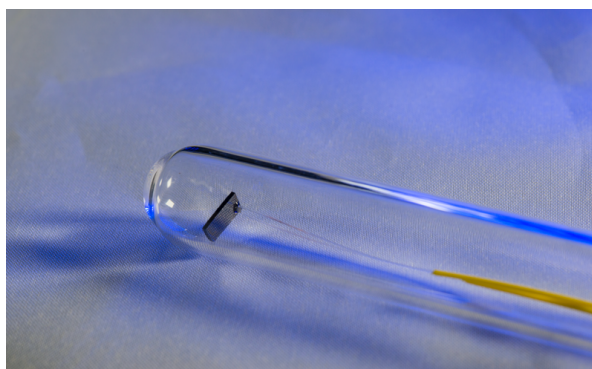


**Figure 5.** Close-up of a photonic thermometer prototype at NIST, revealing the top of the chip-based sensor.

1 stability over this period. Instead, to assess the long-term stability one has to  
2 rely on the history of many similar thermometers calibrated over the years, which  
3 might be unavailable for the emerging new technology simply because it is new or  
4 because each sensor has a unique behaviour as in the example given in figure 3  
5 above. Incidentally, figure 3 also gives an illustration of the absence of short-term  
6 temperature stability in the high-temperature FBGs (long-term stability is absent as  
7 well [33]). Stability can be also conventionally divided with respect to temperature  
8 and with respect to other factors (e.g. stability to mechanical vibration, radiation  
9 damage, etc.). The latter in thermometers is usually referred to as robustness — a  
10 sought-after quality in the research and development stage. For example, Ahmed *et*  
11 *al* [34] recently demonstrated that silicon photonic thermometers can withstand up  
12 to 1 megagray of  $\gamma$ -radiation without showing any changes in device characteristics  
13 such as peak center, peak width, free spectral range, and temperature sensitivity.

- 14 • *Construction* (or *packaging*) is one of the key factors in the development of  
15 thermometers as there exist two conflicting requirements: exposing the sensor  
16 to a temperature stimulus, while protecting it (and its interface electronics) from  
17 everything else (typically referred to as environmental damage). The resultant  
18 custom packaging (see figure 5) usually involves a compromise between performance  
19 and robustness. As packaging is rarely the focus of sensor development at the  
20 research and development stage, its crucial details are often missing in the available  
21 scientific literature on emerging temperature sensors. Meanwhile, as an example: in  
22 recent studies Dedyulin et al [17] found that inappropriate packaging of fiber-Bragg-  
23 grating thermometers could lead to excessive wavelength drifts at high temperatures  
24 and eventually to sensors failure. Similarly, Klimov et al [19] hypothesized that the  
25 observed thermal hysteresis/ageing of the photonic-crystal-cavity thermometer was  
26 due to residual strain imparted by the epoxy used in packaging.
- 27 • *Typical usage and non-usage of the thermometer* requires matching of the  
28 construction and performance of the new temperature sensor with the application's  
29 requirements and limitations. No application is the same, meaning that the

1 requirements underlying a new temperature sensor can vary greatly from application  
2 to application. For example, for a quantum computer operating at cryogenic  
3 temperatures, a thermometer that is limited to a “few mK temperature range”  
4 is sufficient, whereas in an industry, like oil and gas, the ability to measure  
5 temperature with  $\pm 0.1$  K accuracy in a “problematic environment” is more important.  
6 Lastly, regulated sectors like the defense, aerospace or pharmaceuticals (or for  
7 that matter National Metrology Institutes) will want to see size, uncertainty  
8 and stability to match current industrial (standard) PRT levels. The existing  
9 calibration infrastructure, industry standards and user expectations, based on  
10 existing technology, form additional barriers to wide-spread adoption of a new  
11 technology. As such, any emerging technology will have to not only provide a novel  
12 utility, but will likely have to be backwards compatible with existing infrastructure  
13 e.g. the packaged device footprint will likely be limited to a small diameter ( $\sim 10$  mm)  
14 tube (similar to the existing thermocouples and PRTs). When larger, it may require  
15 significant redesign of existing calibration infrastructure. Similarly, the technology  
16 has to be amenable to automation in order to appeal to a wide range of users from  
17 different skill and educational backgrounds.

18 In the following sections, we provide a general overview of the emerging technologies  
19 at the ascent stage through the lens of the important sensors characteristics, outlined  
20 above. For ease of reference, figures of merit are presented in table 1, and a short summary  
21 of each technique’s advantages and disadvantages is given in table 2. Note: For the sake  
22 of brevity, performance metrics, described above, are replaced in table 1 by their proxies.  
23 Thus, we list expected uncertainty, instead of lengthy discussion on accuracy, temperature  
24 sensitivity, that, when combined with the measurement set-up’s characteristics, will  
25 give resolution, primary technique (or not), instead of full description of oftentimes  
26 complex temperature relationship, etc. Other difficult-to-condense characteristics, such  
27 as construction or typical treatment, are not reflected in the table at all, and thus the  
28 text of the following sections should be consulted for details.

**Table 1.** Comparison of emerging and legacy technologies in thermometry

Technology	Primary	Probe Material	Sensitive Element Size	Anticipated Temp range	Typical Sensitivity	Best Reported Uncertainty <sup>a</sup>	Commercial
JNT	y	conductor <sup>b</sup>	$10^{-3}$ m – $10^{-2}$ m	50 nK – 2500 K	0.06 (nV) <sup>2</sup> /Hz/k $\Omega$ /K	2.7 ppm, 273 K [35]	y
Optical Refraction	y	He/N <sub>2</sub>	$10^{-3}$ m – $10^{-1}$ m	100 K – 420 K	3 pm/K	12 ppm, 293 K [36]	n
On-chip DBT	y	Rb/Cs	$10^{-10}$ m <sup>3</sup>	300 K – 1000 K	0.8 Hz/Torr/K	71 ppm, 296 K [37]	n
Optomechanics	y	Si <sub>3</sub> N <sub>4</sub>	$10^{-4}$ m – $10^{-3}$ m	0.05 K – 300 K	0.25 %/K	7.5%, 40 K [38]	n
Phosphor Thermometry	n	ceramic <sup>c</sup>	$10^{-7}$ m – $10^{-2}$ m	<77 K – 2000 K	0.5 %/K	860 ppm, 673 K [39]	y
FBG	n	SiO <sub>2</sub> <sup>d</sup>	$10^{-4}$ m – $10^{-2}$ m	80 K – 1300 K	10 pm/K <sup>e</sup>	610 ppm, 393 K [13]	y
Rayleigh Scattering	n	SiO <sub>2</sub>	$10^{-4}$ m – $10^2$ m	250 K – 470 K <sup>e</sup>	6.67 GHz / K	n/a <sup>f</sup>	y
Brillouin Scattering	n	SiO <sub>2</sub>	$10^{-1}$ m – $10^2$ m	250 K – 350 K <sup>g</sup>	1 MHz/K	n/a <sup>f</sup>	y
Raman Scattering	y	SiO <sub>2</sub>	$10^{-3}$ m – 10 m	250 K – 350 K	n/a	n/a <sup>f</sup>	y
Ring Resonator and Photonic Crystal Cavity	n	Si/Si <sub>3</sub> N <sub>4</sub> <sup>h</sup>	$10^{-4}$ m – $10^{-3}$ m	3 K – 1000 K	80 pm/K <sup>d</sup>	510 ppm <sup>i</sup> , 343 K [19]	n
Long-Stem SPRT	n	Pt	$5 \times 10^{-2}$ m	75 K – 950 K	0.1 $\Omega$ /K	0.04 ppm, 273 K [40]	y
Type S Thermocouple	n	Pt(Rh)	$5 \times 10^{-1}$ m – 1 m	300 K – 2000 K	10 $\mu$ V/K	65 ppm, 693 K [41]	y

<sup>a</sup> Relative uncertainties are usually expressed in an abbreviated form, as parts per million (“ppm”) or parts per hundred (“%”), for example, a 1 ppm =  $1 \times 10^{-6}$  relative uncertainty at 300 K would correspond to  $1 \mu\text{K K}^{-1} \times 300 \text{ K} = 300 \mu\text{K}$ .

<sup>b</sup> Sensors don’t need to be metallic conductors, e.g. electrolytic solutions, graphite rope and plasma of combustion process were used as sensors.

<sup>c</sup> Thermographic phosphors, e.g. Mg<sub>4</sub>FGeO<sub>6</sub>, Al<sub>2</sub>O<sub>3</sub>:Cr

<sup>d</sup> Alternative materials such as sapphire (Al<sub>2</sub>O<sub>3</sub>) or polymers (PMMA) could be used, in which case the temperature range and the size of the sensitive element changes.

<sup>e</sup> Typical resolution of a tunable laser used for interrogation is 0.1 pm. Note: at 1550 nm 80 pm is approximately 10 GHz.

<sup>f</sup> As discussed in detail in section 4.2 the existing work on distributed temperature sensors report on temperature resolution only.

<sup>g</sup> The range can be potentially extended to 1 K – 1100 K.

<sup>h</sup> Other possible materials include SiC, InP, GaAs, Ge, sapphire and diamond.

<sup>i</sup> The unpackaged ring resonator was shown to have an uncertainty of 28 ppm at 363 K [23].

**Table 2.** Advantages and drawbacks of emerging technologies described in Table 1

Technology	Advantages	Drawbacks
JNT	<ul style="list-style-type: none"> <li>✓ Measures thermodynamic temperature (traceable to ohm and second)</li> <li>✓ High absolute accuracy</li> <li>✓ Material independent</li> </ul>	<ul style="list-style-type: none"> <li>× Very small signal levels involved, complex electronic processing</li> <li>× Sensitive to other noise sources, EMI</li> <li>× Long measurement times for high accuracy</li> </ul>
Optical Refraction	<ul style="list-style-type: none"> <li>✓ Measures thermodynamic temperature (traceable to second and pascal)</li> </ul>	<ul style="list-style-type: none"> <li>× Centimeter scale footprint</li> <li>× Susceptible to chemical contamination of working gas</li> <li>× Limited to temperatures below 150 °C (mirror coating)</li> </ul>
On-chip DBT	<ul style="list-style-type: none"> <li>✓ Measures thermodynamic temperature (traceable to second)</li> </ul>	<ul style="list-style-type: none"> <li>× Susceptible to magnetic field</li> </ul>
Phosphor thermometry	<ul style="list-style-type: none"> <li>✓ some phosphors shown to be resistant to ionizing radiation, immunity to EMI and chemical corrosion</li> <li>✓ Many thermographic phosphors available covering a wide temperature range</li> </ul>	<ul style="list-style-type: none"> <li>× Requires calibration (due to batch-to-batch variability, host matrix influence)</li> <li>× Reproducibility of the phosphor coating needs to be improved</li> </ul>
FBG	<ul style="list-style-type: none"> <li>✓ Packaging can be made compatible with the existing calibration infrastructure</li> <li>✓ Point-like temperature sensor</li> <li>✓ Multi-point sensing capability (signal multiplexing)</li> <li>✓ Suitable for static and dynamic measurements (up to kHz)</li> </ul>	<ul style="list-style-type: none"> <li>× Thermal hysteresis, long-term drifts are not well understood</li> <li>× Susceptible to ionizing radiation</li> <li>× Cross-sensitivity (stress, humidity)</li> </ul>
Rayleigh, Brillouin and Raman scattering	<ul style="list-style-type: none"> <li>✓ Distributed temperature sensing, spatial range covers several orders of magnitude (m to 100 km)</li> <li>✓ Resistant to ionizing radiation, immunity to EMI and chemical corrosion</li> <li>✓ Measures thermodynamic temperature (Raman + single photon detector)</li> </ul>	<ul style="list-style-type: none"> <li>× Existing temperature calibration infrastructure and language are not suited for distributed temperature sensing</li> <li>× Susceptible to strain; special device handling and installation protocol are necessary</li> <li>× Detection systems are often complex and expensive (increased training time)</li> </ul>
Ring resonator and photonic crystal cavity	<ul style="list-style-type: none"> <li>✓ Wide range of materials, wavelengths and device design parameters available for fit-for-purpose device development</li> <li>✓ Resistant to chemical contamination</li> <li>✓ Lowest uncertainties compared to other defined-scale techniques</li> </ul>	<ul style="list-style-type: none"> <li>× Low drift packaging needs to be developed</li> <li>× Susceptible to manufacturing imperfections</li> </ul>
Optomechanics	<ul style="list-style-type: none"> <li>✓ On-chip thermodynamic temperature</li> <li>✓ Integrateable with on-chip photonic thermometers</li> </ul>	<ul style="list-style-type: none"> <li>× Early stage of research</li> <li>× Uncertainties estimated to be on the order of 1 K or higher</li> <li>× Requires high vacuum</li> </ul>

### 3. Emerging technologies for primary thermometry

On 20 May 2019 a revision of the International System of Units (the SI), agreed by the General Conference on Weights and Measures, came into force [42–44]. The new definition of the kelvin is based upon the Boltzmann constant,  $k_{\text{B}} = 1.380649 \times 10^{-23} \text{ JK}^{-1}$  — a factor that converts thermodynamic temperature to energy. In the route towards the re-definition, a whole host of national metrology institutes worked diligently to produce the most accurate measurements of the Boltzmann constant (the Boltzmann project [45]), using acoustic gas thermometry [7], Johnson noise thermometry [8], dielectric constant gas thermometry (DCGT [46]) and Doppler broadening thermometry (DBT [47]), to name a few. Three of them — AGT, DCGT and JNT — were utilized for the final CODATA  $k_{\text{B}}$  value [48]. It is this effort that in part motivated the development of the primary technologies, described below. If previously, for the Boltzmann constant measurements, the experimenters would determine  $k_{\text{B}}$  from  $k_{\text{B}} = F/T_{\text{TPW}}$ , where  $F$  is an experimental quantity measured in joules and  $T_{\text{TPW}}$  is the temperature of the triple point of water, which was set equal to 273.16 K, now, for primary temperature realization, this relationship is inverted, and thermodynamic temperature  $T$  can be found from the same experiment, using the CODATA value for  $k_{\text{B}}$ .

Most, if not all, of the primary thermometry techniques will be familiar to the temperature metrology community. Technical details for some of them have been covered in multiple review articles and those which are sufficiently mature to provide traceability<sup>‡</sup> to the kelvin with low uncertainties, are described in the *Mise en pratique* for the definition of the kelvin [6]. Here our interest is limited to a subset of primary techniques that are either actively commercialised, or are generally considered to be strong candidates for commercialization in the near future. The following discussion provides a brief technical background of each technique, followed by evaluation of the prospects of each technique, entering the mainstream user market and their potential impact.

#### 3.1. Johnson noise thermometry

Johnson noise thermometers determine the thermodynamic temperature from measurements of the fluctuating voltage or current noise, caused by the thermal motion of electrons that occurs in all electrical conductors [8, 50, 51]. Usually, Johnson noise is characterized by its mean-square voltage,  $\overline{V_{\text{T}}^2}$ , conventionally called the noise power. For temperatures above 25 K and frequencies below 1 MHz, the noise power is approximated with a relative error of less than 1 ppm by Nyquist’s law:

$$\overline{V_{\text{T}}^2} = 4k_{\text{B}}T\Re(Z)\Delta f,$$

where  $\Delta f$  is the bandwidth over which the noise voltage is measured,  $\Re(Z)$  is the real part

<sup>‡</sup> Metrological traceability refers to a property of a measurement result whereby the result can be related to a reference (which can be a practical realization of a measurement unit), through a documented unbroken chain of calibrations, each contributing to the measurement uncertainty [49].

1 of the conductor impedance  $Z$ , and  $T$  is the thermodynamic temperature [52, 53]. From  
 2 this equation, thermodynamic temperature can be determined directly by measuring the  
 3 fluctuating voltage across a sensing resistor and using the CODATA value for  $k_B$  (see  
 4 introduction to section 3). Because the gain and bandwidth of the noise thermometer in  
 5 Nyquist’s law above can be difficult to quantify precisely, in most of JNT measurement  
 6 schemes, the temperature is calculated using relative measurement instead, from the  
 7 ratio of the measured noise powers — of which one with a resistor at the unknown  
 8 temperature, and another with a reference noise source. Usually the reference noise  
 9 source is a resistor at a known temperature, but shot noise from diodes, multi-resistor  
 10 and thermistor networks, and synthetic noise sources have also been used [8].

11 The minimum uncertainty in the absolute JNT temperature measurement is given  
 12 by Rice’s equation [54]:

$$13 \quad \frac{u(T)}{T} \Big|_{\min} = \left( \frac{1}{\tau \Delta f} \right)^{1/2}$$

14 where  $\tau$  is the measurement period. Note: For the relative measurement, the minimum  
 15 relative uncertainty is four times the value given by Rice’s formula. The expression  
 16 above highlights one of the major drawbacks of JNT: large amounts of data/time are  
 17 required to make accurate measurements of a small (random) signal. For example, the  
 18 highest accuracy JNT measurements (of Boltzmann constant) to date [35] with a relative  
 19 standard uncertainty of 2.7 ppm required the integration time of 100 days and the  
 20 amount of total data acquired exceeded 100 TB. At its best, such a thermometer could  
 21 measure just three temperatures per year!

22 One of the main attractions of JNT (apart from measuring thermodynamic  
 23 temperature) is that so long as the sensor resistance can be measured, the noise power  
 24 expression above is insensitive to chemical, mechanical and even ionizing-radiation-  
 25 induced changes in the sensor: no other sensor has such immunity to material changes.  
 26 Noise thermometry has been successfully applied at temperatures ranging from below 50  
 27 nK to 2473 K [51, 55], a range far exceeding that of any other temperature sensor. The  
 28 electronic nature of JNT means that the sensors can be easily interfaced with existing  
 29 electrical measurement infrastructure. However, the challenges involved in measuring  
 30 such a small signal accurately, quickly and in the presence of other noise sources mean  
 31 that noise thermometry is not a practical option for most applications. JNT is unlikely  
 32 to be adopted as a routine industrial technique until measurement uncertainties of 0.1 %  
 33 or less can be obtained in a few seconds. At present only three JNT techniques meet the  
 34 industrial need with respect to speed [8]:

- 35 • The superposition thermometer, which operates close to the limit, prescribed by  
 36 Rice’s equation, combines a high statistical efficiency with a bandwidth of 1 MHz,
- 37 • The dual noise thermometer that combines a noise thermometer with a much faster  
 38 conventional thermometer, either a resistance thermometer or thermocouple,
- 39 • Very wide-band radio-frequency noise thermometer, for which the measurement  
 40 uncertainty is limited to about 1 % by amplifier noise and uncertainties, associated

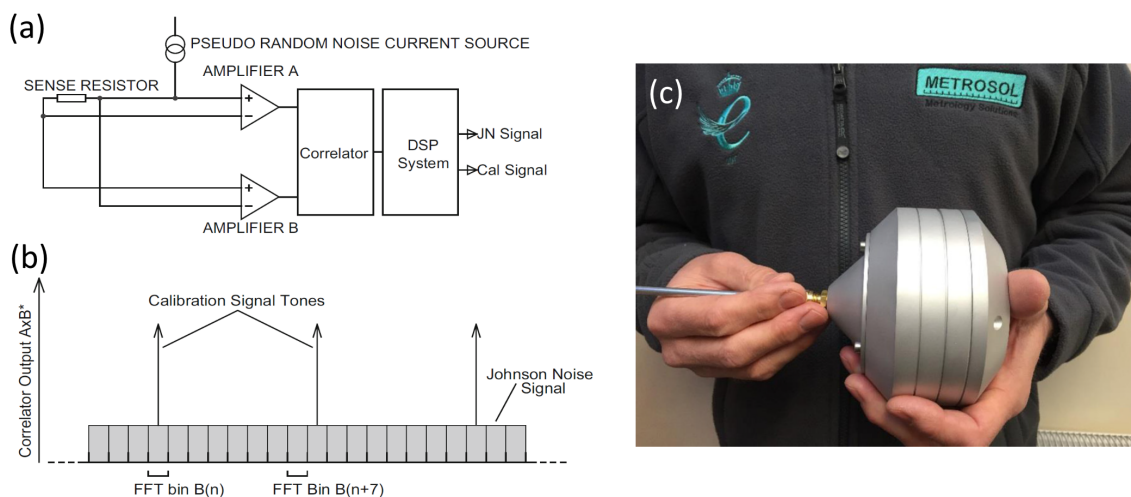


**Figure 6.** (a) A simplified schematic diagram of a superposition thermometer using pseudo random current injection which can be separated from Johnson noise in the frequency domain. (b) Correlator output from Metrosol's JNT system. In reality, the calibration tones are 30 dB larger than the Johnson noise (reproduced from [57]). (c) Metrosol's JNT2 prototype of the superposition thermometer (reproduced from [58]).

1 with the measurement and calibration of noise powers.

2 One of the aforementioned techniques, the superposition thermometer, has been  
 3 commercially developed by Metrosol§ in collaboration with the National Physical  
 4 Laboratory (NPL), UK (see figure 6) [56–58]. It uses pseudo random current injection  
 5 for the calibration signal, which can be separated from Johnson noise in the frequency  
 6 domain. The system is relatively compact (16 cm<sup>3</sup>), shows immunity to external EMI,  
 7 and at 293 K with a 1.2 MHz bandwidth over a measurement time of just over 6.5 s  
 8 the reported standard deviation is 0.232 K [58]. Further work needs to be done to  
 9 characterize the ultimate performance/uncertainties. Development of a JNT with 100  
 10 mK-level accuracy will be broadly useful for the metrology community replacing a  
 11 desperate range of ITS-90 artefacts with a singular measurement apparatus, lower cost  
 12 of disseminating and maintaining the kelvin.

### 13 3.2. Optical cavities and gas refractivity measurements

14 Following the footsteps of pioneering work in acoustic gas thermometry [7], several  
 15 laser-based interferometry techniques are under study to interrogate the thermodynamic  
 16 temperature of a gas through an equation-of-state approach. In the refractivity-based  
 17 approach, the underlying physical phenomenon is concerned with how the change in  
 18 density impacts the polarizability of the gas [36, 59, 60]. In this method, the gas density

§ Disclaimer: Certain equipment manufacturers are identified in this paper with regards to commercialization of primary thermometry techniques. Such identification is not intended to imply endorsement by the authors or the institute they are affiliated with.

1 ( $\rho$ ), pressure ( $P$ ) and thermodynamic temperature ( $T$ ) are related through the virial  
2 equation of state:

$$3 \quad P = k_{\text{B}}T(\rho + B_{\rho}\rho^2 + C_{\rho}\rho^3 + \dots)$$

4 where the deviations from the ideal gas law are considered by density virial coefficients  
5  $B_{\rho}$  and  $C_{\rho}$ . The density of gas,  $\rho$ , can be determined by combining experimental  
6 measurements of gas refractivity,  $(n - 1)$ , with theoretical calculations using the  
7 Lorentz–Lorenz equation [36]:

$$\rho = \frac{2}{3A_{\text{R}}}(n - 1) + \frac{A_{\text{R}} + 4B_{\text{R}}}{9A_{\text{R}}^2}(n - 1)^2 + \\ + \frac{4(A_{\text{R}}^4 - 4B_{\text{R}} - A_{\text{R}}^3 * B_{\text{R}} + 2A_{\text{R}} * C_{\text{R}})}{27A_{\text{R}}^5}(n - 1)^3 + \dots$$

8 where the refractivity virial coefficients  $A_{\text{R}}$ ,  $B_{\text{R}}$  and  $C_{\text{R}}$  depend upon the polarizability  
9 and the diamagnetic susceptibility of the gas, and the frequency of the light being  
10 refracted. In order to determine the thermodynamic temperature in a refractivity-based  
11 measurement scheme one needs to combine a measurement of the pressure  $P$  by an  
12 independent method (e.g. by using a piston gauge) together with the CODATA value for  
13  $k_{\text{B}}$  (see introduction to section 3). Insufficient knowledge of the higher virial coefficients  
14 of all other gases has historically limited most primary measurements to using helium  
15 (He) as the working gas [59]. Unfortunately, helium only weakly refracts light, so the  
16 measurement is very sensitive to uncertainties from apparatus distortions (i.e. distortion  
17 of the cavity walls due to gas absorption, linear expansion of ultra-low expansion glass,  
18 used in device construction, gas pressure-dependent distortion of the mirror) and from  
19 the chemical purity of the gas [59]. There have been on-going efforts to address these  
20 issues in the context of pressure metrology that will no doubt positively impact any  
21 future deployment of such an approach for the realization of  $T$  [36, 61, 62].

22 Relative primary measurements, that use non-helium working gases, have been  
23 demonstrated with some trade-offs to accuracy [59]. Recently, Ricker *et al* [63]  
24 evaluated the potential feasibility of the fixed length optical cavity (FLOC) approach for  
25 thermometry. The FLOC approach, pioneered by the National Institute of Standards  
26 and Technology (NIST), USA is based upon a dual-cavity Fabry-Perot refractometer  
27 (see figure 7) that has been used as a pressure transfer standard, traceable to a mercury  
28 manometer [60] and was recently commercialized by MKS Instruments [64]. In the  
29 proposed future application of FLOC for temperature measurements, Ricker *et al*  
30 projected a combined standard uncertainty of 1.5 mK (or 5.0 ppm in relative terms)  
31 at 300 K, dominated by the uncertainty in the refractivity of the nitrogen ( $\text{N}_2$ ) gas  
32 to be used for the envisioned implementation. Replacing  $\text{N}_2$  with helium (He) gas  
33 should improve the accuracy, however the temperature sensitivity would substantially  
34 decrease [63]. The approach, proposed by Ricker *et al* has several outstanding issues  
35 that need to be resolved (as described in sections 3.3 and 5.1 of [59]). For example, if  $\text{N}_2$   
36 is used,  $A_{\text{R}}$  is a temperature-dependent constant [59]; since  $A_{\text{R}}$  is present in the FLOC

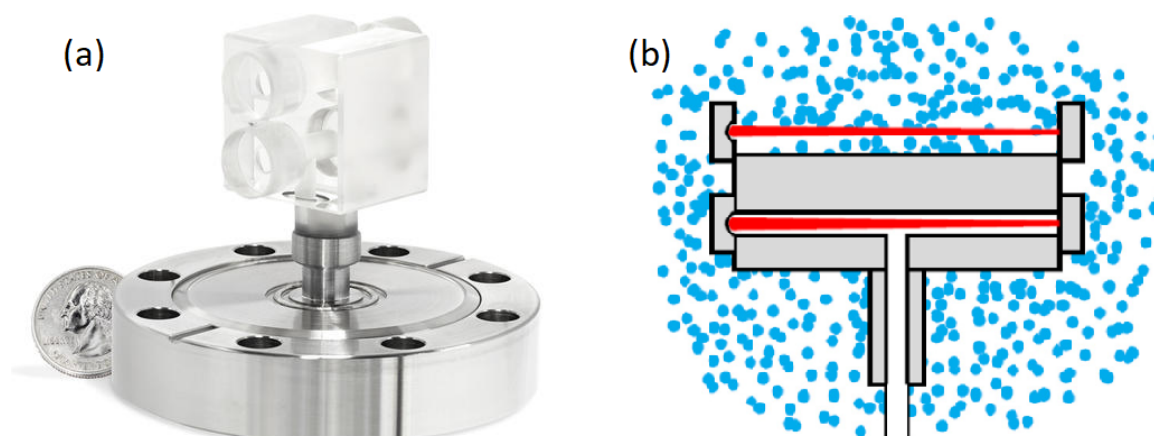


**Figure 7.** (a) The image of the prototype FLOC laser cavity at NIST that could be used for temperature measurements. (b) The schematic of the FLOC laser cavities. The upper cavity is allowed to interact with gas molecules (represented with dots) and the lower cavity is at vacuum ( $< 1$  mPa) (reproduced from [63]).

1 working equation above at first order, such a device would not satisfy the definition of a  
 2 primary thermometer from the *Mise en pratique* (see section 1 above).

3 A chief drawback or limitation of the FLOC approach is its macroscopic footprint,  
 4 which though significantly smaller than acoustic gas thermometers, is still orders of  
 5 magnitude larger than that, associated with a resistance thermometer. Furthermore,  
 6 the upper limit to the temperature measurement range will be limited by the thermal  
 7 stability of mirror coatings, which is often limited to temperatures below 430 K, whilst  
 8 the lower temperature limit is set by the de-sublimation/pre-condensation temperature  
 9 of the gas. Finally, waiting times required to reduce temperature gradients present after  
 10 filling to pressure (1 h in [63]) will limit the use of the method in dynamic-measurement  
 11 settings. It is likely that such devices will find specialized use in metrology labs, where  
 12 they can provide an accessible route to thermodynamic temperature. A particularly  
 13 attractive option for metrology labs would be the ability to utilize a common platform  
 14 to realize both pressure and temperature (although not simultaneously), thus providing  
 15 a resource-efficient pathway to building new measurement capabilities.

### 16 3.3. Doppler-line broadening thermometry

17 The principle of DBT is to record the Doppler profile of a molecular (or atomic) absorption  
 18 line of a gas in thermodynamic equilibrium [47, 65] (see figure 8). The absorption line  
 19 shape of single rotational-vibrational (rovibrational) molecular line is dominated at very  
 20 low pressure by Doppler broadening and is a simple Gaussian profile, which reflects  
 21 the Maxwell-Boltzmann velocity distribution of gas particles along the laser beam axis.  
 22 In practice however, collisions, speed-dependent and Lamb-Dicke-Mössbauer narrowing  
 23 effects lead to a different profile of the gas absorption line. In conjunction with some

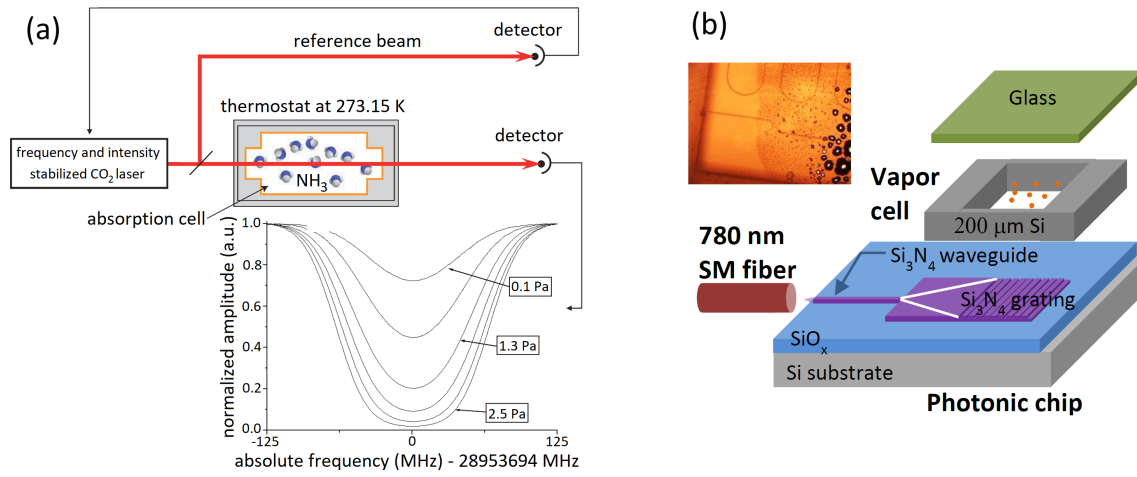


**Figure 8.** (a) The Doppler Broadening Technique principle (adapted from [70]) (b) Design for photonic coupled alkali vapor cell on a chip. Inset: first such vapor cell fabricated at NIST showing SiN waveguides and alkali atom droplets condensed on the inside wall of the cell (reproduced from [71]).

- 1 highly accurate modeling of the line profile, it is possible to use the data to retrieve the
- 2 Doppler half-width at half-maximum,  $\Delta\nu_D$ , using the following equation [65]:

$$3 \quad \Delta\nu_D = \frac{\nu_0}{c} \sqrt{2 \ln 2 \frac{k_B T}{M}}$$

- 4 where  $\nu_0$  is the line-center frequency,  $c$  is the speed of light, and  $M$  is the absorber mass.
- 5 From this equation, the thermodynamic temperature of a gas (e.g.  $\text{NH}_3$ ,  $\text{CO}_2$ ,  $\text{C}_2\text{H}_2$ )
- 6 can be retrieved using the CODATA value for  $k_B$  (see introduction to section 3).

7 The use of Doppler broadening for thermometry, as opposed to determining the  
 8 Boltzmann constant [45, 66], has been pursued by various National Metrology Institutes  
 9 (NMIs), including as part of EURAMET’s “Implementing the new kelvin 2” (InK2)  
 10 project [67]. Recent published results from that work [68] with acetylene ( $\text{C}_2\text{H}_2$ ) at  
 11 the triple point of water and the gallium melting point gave a combined uncertainty  
 12 of 7 mK (23 ppm in relative terms) with a largest contribution coming from statistical  
 13 reproducibility, which could be further reduced in the future [68].

14 A practical DBT is currently facing two main challenges: a high level of ancillary  
 15 equipment (and the associated cost and power requirements) currently needed to drive  
 16 the technique and the scale of the “sensing element”. The first challenge stems from an  
 17 ever present requirement for high signal to noise ratio in lineshape measurement and the  
 18 need to accurately and reproducibly measure the frequency of the laser. The solution for  
 19 this is (potentially) a matter of engineering. The second challenge refers to the fact that  
 20 most of the DBT research has been undertaken in macroscopic optical cells, which makes  
 21 it unattractive for industrial use. The exception to this is the use of small cm-scale gas  
 22 cells containing metallic vapor such as Cs [37, 69]. To overcome the second challenge  
 23 requires a further down-scaling of the “sensing element” whilst retaining the essential  
 24 requirement of adequate thermalization of the gas/vapor within the cell itself.

1 A promising avenue is the use of on-chip integrated vapour cells, currently being  
 2 developed for atom-based quantum sensing applications [71] (see figure 8). In one  
 3 implementation, the device fabrication utilizes fiber coupled grating couplers to deliver  
 4 and collect light from the vapour cell. Alternatively, leaky waveguides (e.g. slot  
 5 waveguides and photonic crystal waveguides) or a resonator's evanescent field have  
 6 been used to probe the gas molecules near the photonic structures [72]. Either  
 7 implementation however, will have to overcome several technical challenges for these  
 8 devices, to prove being competitive, including: non-linear/complex baseline due to  
 9 waveguide backscattering or grating/vapor cell etalon, lineshape changes due to boundary  
 10 effects at the device-air interface (for the case of evanescent field based sensing) and  
 11 magnetic field compensation for atomic vapor cells. The principle advantage of a fiber-  
 12 coupled vapour-cell based DBT would be the same form-factor and a similar temperature  
 13 range as for an industrial resistance thermometer, which means that no alterations to  
 14 the existing physical infrastructure will be required.

### 15 3.4. Optomechanical thermometry

16 Optomechanics is the study of interaction between the optical field and the mechanical  
 17 motion of an optical element via radiation pressure [73]. In a typical implementation  
 18 the (nano)mechanical resonator is driven to vibrate randomly by thermal forces from its  
 19 environment in a band of frequencies around its mechanical resonance. This mechanical  
 20 motion creates high- and low-frequency sidebands (anti-Stokes and Stokes shift; see  
 21 figure 9a) around the optical field frequency due to the Doppler effect (this is essentially  
 22 the same process as Raman scattering) [38, 74, 76]. In addition, the random, quantum  
 23 intensity fluctuations of the probe optical field drive the mechanics with so-called radiation  
 24 pressure shot noise (quantum measurement backaction). The motion from backaction  
 25 is also imprinted as phase fluctuations on the output light, establishing a quantum  
 26 correlation between amplitude and phase fluctuations of the optical mode. The quantum  
 27 correlations manifest themselves as an asymmetry between the Stokes and anti-Stokes  
 28 side bands [38, 77]. In Raman-ratio thermometry the ratio of Stokes to anti-Stokes  
 29 Raman transition is equal to [74]:

$$30 R_{\text{sa}} = e^{\hbar\omega_m/k_B T} = (\bar{n} + 1)/\bar{n}$$

31 where  $\omega_m$  is the mechanical resonance frequency. The spectrum of Raman scattered light  
 32 transmitted through an optomechanical cavity is given by [74]:

$$33 S(\omega) \propto \frac{\bar{n}}{(\frac{\Gamma_m}{2})^2 + (\omega_m - \omega)^2} + \frac{\bar{n} + 1}{(\frac{\Gamma_m}{2})^2 + (\omega_m + \omega)^2}$$

34 This expression holds when the laser is resonant with the optical cavity, and the optical  
 35 cavity linewidth is much larger than the mechanical linewidth  $\Gamma_m$ . The first (second)  
 36 term corresponds to the anti-Stokes (Stokes) scattering peak shifted by  $\omega_m$  ( $-\omega_m$ ) from  
 37 the input laser frequency, and  $\omega$  is the frequency relative to the input laser frequency.  
 38 Taking the ratio of the amplitude of the Stokes and anti-Stokes peaks directly yields the

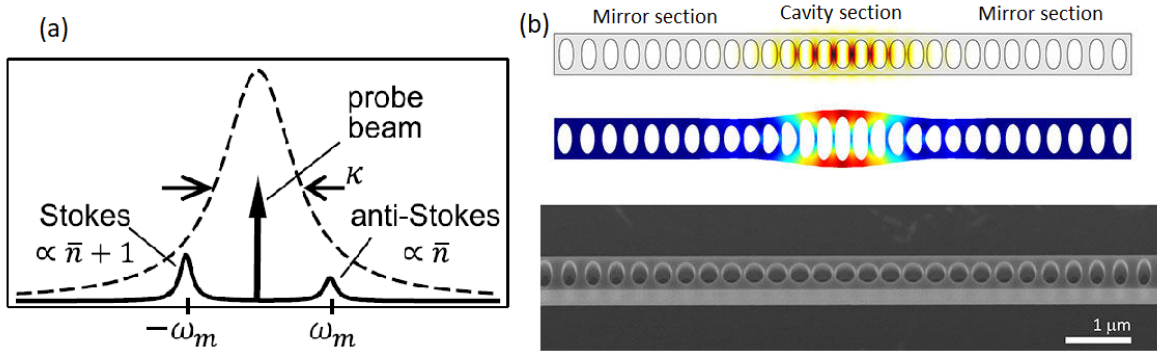


**Figure 9.** (a) The spectrum of transmitted probe beam light shows Raman scattering peaks shifted by  $\pm\omega_m$ , where  $\omega_m$  is the mechanical resonance frequency. The asymmetry in the spectral peaks, dependent on the effective thermal occupation of the mechanical mode, forms the basis for a temperature measurement. Also indicated is the spectral response of the optical cavity (dashed curve) (reproduced from [74]). (b) Top: Scheme of optomechanical crystal geometry, overlaid with a simulation of an optical resonance. Middle: Scheme showing a mechanical breathing mode. Bottom: Scanning electron photograph of a silicon optomechanical crystal.

1 mechanical occupation,  $\bar{n} = 1/(R_{sa} - 1)$  and the temperature can be found using the  
 2 expression for  $R_{sa}$  above.

3 This method has been utilized by Purdy *et al* to measure thermodynamic  
 4 temperature of nano-mechanical devices over the temperature range of 0.5 mK up to 50  
 5 K [74]. More recently quantum cross-correlation technique, probing side band asymmetry,  
 6 has been employed by Purdy *et al* to enable temperature measurements up to 300 K [38].  
 7 Using free standing silicon nitride (SiN) membranes in high vacuum, Ferreiro-Vila *et al* [75]  
 8 have demonstrated room temperature thermometry with 15  $\mu$ K resolution. At present, the  
 9 reported uncertainties in optomechanical temperature measurements are of the order of  
 10 ten percent [38] which is too large for any but niche applications at very low temperatures.  
 11 The on-chip design of optomechanical thermometers and thus their ability to integrate  
 12 with existing silicon photonics and electronics infrastructure, particularly in the context  
 13 of quantum computing, is certainly an attractive feature. In order to realize a practical  
 14 optomechanical primary thermometer with acceptable uncertainty, several challenges,  
 15 however, must be overcome including optimization of optomechanical transduction,  
 16 developing robust vacuum-compatible packaging, characterization of systematic effects  
 17 such as self-heating, optical bistability, cavity chaos and characterization of energy flow  
 18 between the bath and mechanical modes of the resonator [78].

19 The quest to optimize optomechanical transduction has driven a continuous evolution  
 20 of optomechanical sensor's design from simple disk resonators to complex designs featuring  
 21 coupled photonic crystal cavities in a "zipper" configuration shielded from its surrounding  
 22 by an integrated microfabricated phononic shield [79]. In recent years, the material  
 23 of choice has evolved from silicon to silicon nitride, enabling higher Q devices. Use of  
 24 hierarchical design features has recently enabled the fabrication of silicon nitride devices

1 with mechanical Q's of up to a billion [80]. Fabrication techniques have made novel  
 2 materials such as diamond, gallium arsenide (GaAs) and aluminium nitride (AlN) more  
 3 readily available, opening up new paths to realizing optomechanical sensors with an  
 4 optomechanical coupling rate of 100 GHz/nm [81]. More recently, the use of metamaterial  
 5 design elements in fabricating optomechanical resonators [82] has enabled mechanical  
 6 Q's of nearly one thousand in structures where the buried oxide layer is not etched  
 7 out. Such structures are easier to fabricate in large numbers, requiring fewer post-  
 8 foundry modifications, if any, and likely to prove more robust against internal strain and  
 9 mechanical vibrations from the environment.

#### 10 **4. Emerging technologies for approximations of defined scales**

11 Emerging technologies for approximations of defined scales could be divided into two  
 12 broad categories: fiber-optic based temperature sensors — that use optical fibers, either  
 13 to guide the light to and from the sensor (e.g. phosphor thermometry), or as a sensing  
 14 element itself (e.g. fiber Bragg gratings, Brillouin thermometry) — or fiber-coupled  
 15 on-chip thermometers — that use on-chip nanophotonic devices to sense temperature  
 16 changes.

17 Given that fiber-optic technology has been well established for over half a century [83]  
 18 it is not surprising that many researchers have tried to harness guided light to measure  
 19 physical quantities such as temperature, pressure and humidity [84,85]. Fiber-optic sensor  
 20 technology has benefited from the rapid developments in closely related optoelectronic  
 21 and fiber-optic communications industries, as component prices have fallen and quality  
 22 improved, the ability of fiber-optic sensors to displace traditional sensors has grown.  
 23 The most common fiber-based temperature sensing device is the fiber Bragg grating  
 24 (FBG) [86,87] though other examples, as demonstrated in the literature, include long-  
 25 period gratings [88], extrinsic Fabry-Perot cavities [89,90], microloop resonators [91]  
 26 and light scattering-based fiber thermometers, including Brillouin, Rayleigh [92] and  
 27 Raman [93] fiber thermometers. These fiber thermometers provide convenient access to  
 28 either primary (see section 4.2) or ITS-90 traceable measurement solutions.

29 The fundamental limitations of various silica fiber-optic techniques such as  
 30 uncertainty performance (phosphor thermometry in section 4.1, FBG in section 4.3),  
 31 stability (FBG in section 4.3), and inadequate spatial, temporal and thermal measurement  
 32 resolution (Brillouin scattering in section 4.2) can be overcome by utilizing on-chip  
 33 nanophotonic, devices where strong confinement of light combined with higher TOC  
 34 materials can be used to realize a variety of devices ranging from coarse but stable  
 35 temperature sensors (e.g. Bragg-waveguide-grating thermometers [94]) to high resolution,  
 36 low-drift thermometers (e.g. ring resonators [21,26]). Consider, for example, the most  
 37 common material in the semiconductor industry — silicon. It has a thermo-optic  
 38 coefficient 10 times larger than that of silica ( $\sim 1 \times 10^{-4} \text{ K}^{-1}$  [95] vs.  $\sim 1 \times 10^{-5}$   
 39  $\text{K}^{-1}$  [96]) — thus a greater temperature sensitivity (up to a factor of ten higher) is  
 40 achievable. Pure single crystal Si suitable for integrated optics is readily available in

1 the form of silicon-on-insulator (SOI) wafers. The Si waveguide devices are normally  
2 embedded in a SiO<sub>2</sub> cladding and therefore isolated from contamination, further oxidation  
3 and potential drift. Si photonic thermometers could theoretically be used from cryogenic  
4 temperatures up to the glass transition temperature of the SiO<sub>2</sub> cladding, which can be  
5 over 1000 K for pure SiO<sub>2</sub> layers. Such devices can be less than 100 μm in size, while the  
6 underlying Si chip is typically a few millimeters across to facilitate mechanical handling.

7 Below we provide a brief overview of some of the more common fiber-optic based  
8 technologies followed by the on-chip technologies.

#### 9 4.1. Fiber-coupled phosphor thermometry

10 Phosphor thermometry and in particular fiber-coupled phosphor thermometry has  
11 been the subject of intense research for many years and there are a number of good  
12 introductions to the subject [97–101]. Phosphor thermometry is based, in essence, on  
13 photoluminescence — the emission of light at one wavelength caused by excitation at  
14 a different wavelength — of a particular class of ceramics known as thermographic  
15 phosphors (e.g. Mg<sub>4</sub>FGeO<sub>6</sub>:Mn (MFG) and Al<sub>2</sub>O<sub>3</sub>:Cr (Ruby) [97, 98]) that are either  
16 applied to the surface of interest or embedded in an optical fiber. In the latter case,  
17 phosphorescent light from the material coated on the end of the fiber is efficiently back  
18 propagated by the fiber while in the former case a co-located fiber is used to collect and  
19 guide the light from a thin (typically 100 μm thick) layer of phosphor to a detector.

20 The collected light is analyzed, using either a decay-time-measurement approach  
21 or a spectral-intensity-ratio-measurement approach. In decay time measurement, the  
22 exponential decay of the emitted fluorescent light is measured after the excitation light is  
23 switched off. The characteristic decay time (typically a few μs to a few ms) of a particular  
24 phosphor is dependent upon its temperature (usually getting smaller with increasing  
25 temperature) and thus the surface temperature can be determined. The decay can either  
26 be measured directly or as a phase difference between a periodically varying excitation and  
27 the corresponding emission [102]. In the case of the spectral-intensity-ratio-measurement  
28 approach, the thermographic phosphor can be excited excited by an external light source;  
29 either pulsed or continuous, and the emission spectrum of the emitted phosphorescent  
30 light is measured. The ratio of two spectral bands in the spectrum of some phosphors has  
31 been found to be temperature dependent and hence can be used as a thermometer [99],  
32 although with a non-linear temperature dependence (see figure 10). Since there is some  
33 batch-to-batch variability in the properties of thermographic phosphor, combined with  
34 the influence of the host matrix, both approaches require calibration to obtain the best  
35 temperature performance (which is very similar for both). For two colour phosphor  
36 thermometry, besides establishing specific temperature traceability to the ITS-90, to get  
37 reliable thermometry performance the optical alignment and other confounding factors  
38 need to be carefully considered, especially for fibre-coupled free space applications

39 Lowe *et al* [103] reported standard uncertainty ranges from 0.6 K at 273 K to 2 K  
40 at 923 K, using phosphor-based fiber-optic thermometer with the spectral intensity ratio

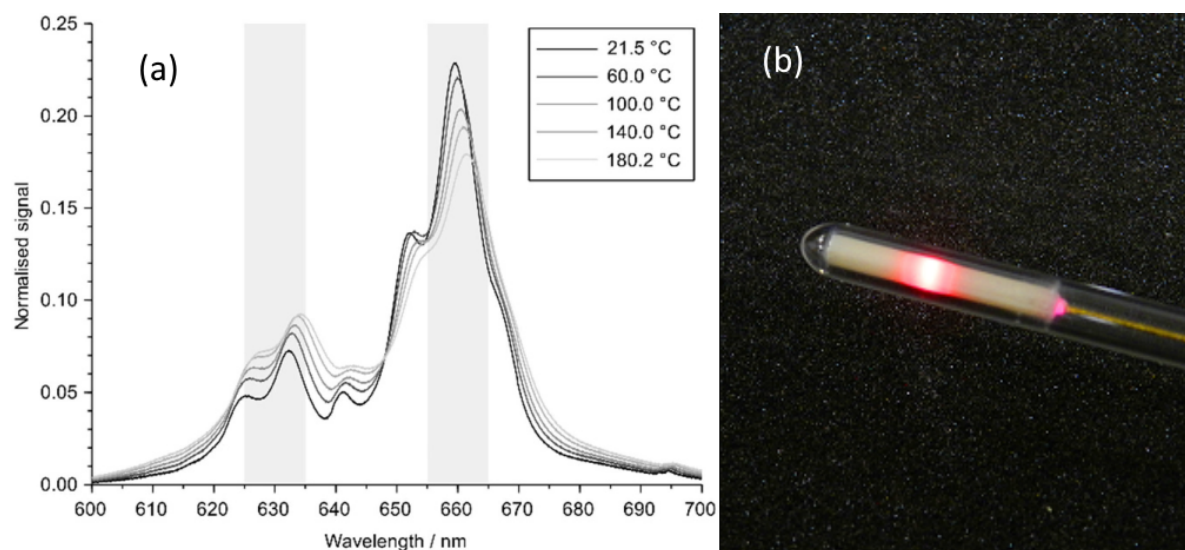


**Figure 10.** (a) Emission spectra of MFG:Mn at different temperatures when excited with light at 415 nm. The shaded areas indicate spectral regions 10 nm bandwidth centered at 630 nm and 660 nm which can be seen to have different temperature dependence (reproduced from [103]). (b) Prototype of a contact phosphor thermometer at work. The MFG:Mn phosphor powder is sealed inside the alumina tube which is bonded to the gold-coated single fiber.

1 approach. The major uncertainty contributions came from repeatability and hysteresis  
 2 of the sensor (it was found that with continued cycling to 923 K the probe started to  
 3 break-up), the interpolation between calibration points and the absolute accuracy of  
 4 the voltage measurement. Similarly, Rosso *et al* [39] reported a standard uncertainty,  
 5 ranging from 0.3 K at ambient temperature to less than 0.7 K at 723 K, using the decay-  
 6 time approach — which is lower than the corresponding uncertainties of a radiation  
 7 thermometer and a K-type thermocouple in their experiments. The major uncertainty  
 8 contributions in their phosphor-thermometry measurement were from the reproducibility  
 9 of the phosphor-coating method, phosphor calibration and repeatability of the decay-time  
 10 estimate.

11 This performance can be further improved by having more calibration points,  
 12 developing a mechanically robust packaging and optimizing phosphor application  
 13 techniques. With care, at modest temperatures, traceable uncertainties of 0.1 K are  
 14 possible — which still might be considered too high for the most accurate applications.  
 15 Nevertheless, phosphor thermometry offers unique advantages in industrial settings,  
 16 especially as regards the surface temperature measurements, since it is independent  
 17 of radiance (so phosphor thermometry can work under water or other transparent  
 18 liquids), independent of surface emissivity and reflected thermal radiation (while radiation  
 19 thermometry approaches are significantly impaired by them) and immune to the presence  
 20 of ionizing radiation or microwave fields. Currently the temperature range for application  
 21 of phosphor thermometry extends from cryogenic temperatures up to almost 2000  
 22 K [104,105]. Using fiber-coupled phosphor thermometry has the advantage of simplifying

1 the experimental set-up and making the form-factor compatible with the existing physical  
2 infrastructure.

### 3 *4.2. Fiber optic thermometry, based on Raman, Brillouin and Rayleigh scattering*

4 Distributed (as opposed to point-like (in section 4.3)) fiber optic sensors measure changes  
5 in the backscattered light over the entire length of an optical fiber. Backscattering is  
6 described as spontaneous when the input light (at a low light-intensity level) is scattered  
7 without strongly altering the property of the medium. In general, the spontaneous  
8 light scattering is a random statistical process occurring in all angular directions and  
9 includes Rayleigh, Brillouin, and Raman scattering in the order of decreasing intensity  
10 (see figure 11). In optical fibers, the scattered light — modulated by local temperature,  
11 strain, vibration and acoustic wave changes — is guided back to the detector over lengths  
12 ranging from meters to hundreds of kilometers [106]. The location of the modulated  
13 signal along the optical fiber can be measured by pulsing the input light and measuring  
14 the time delay of the returning signal — so called optical time-domain reflectometry  
15 (OTDR). In OTDR, the spatial resolution  $\Delta z$  is typically given by [107]:

$$16 \quad \Delta z = \frac{\tau c}{2n_{\text{eff}}},$$

17 where  $\tau$  is the pulse width,  $c$  is the speed of light and  $n_{\text{eff}}$  is the effective refractive index of  
18 the fiber, which is associated with a group index. Alternatively, optical frequency-domain  
19 reflectometry (OFDR) uses a tunable laser to scan a frequency range of  $\Delta F$  and through  
20 Fourier transformation produces a spatial resolution of [107]:

$$21 \quad \Delta z = \frac{c}{2n_{\text{eff}}\Delta F}.$$

22 Improving the spatial resolution (to a few cm level) is the focus of active research  
23 in distributed fiber optic sensors. For information on a large variety of measurement  
24 schemes, both in time and frequency domain, a number of recent review articles can be  
25 consulted [107–109]. The performance of the distributed temperature sensor (DTS) is  
26 a complicated function of the spatial resolution, the temperature resolution, and the  
27 maximum sensing distance, required. The temperature accuracy is typically reduced as  
28 the spatial resolution and sensing distance limit are increased.

29 Rayleigh scattering in optical fibers is caused by the scattering of light from  
30 particles or other sources of refractive index fluctuations much smaller than the optical  
31 wavelength [110]. These density and compositional inhomogeneities are frozen into the  
32 structure of the fiber during fiber fabrication. Rayleigh scattering is an elastic scattering  
33 process— no energy is transferred to the glass matrix — and thus it occurs at the incident  
34 light frequency (see figure 11). For regular silica fibers, the dependence of Rayleigh  
35 scattering intensity on temperature is too weak for use as a temperature sensor [107] and  
36 different materials have to be used instead. For example, liquid core fibers with OTDR  
37 instrumentation were predicted to have an accuracy of 1 K with a spatial resolution of a  
38 few meters over 100 m fiber length [111]. Alternatively, the temperature information can

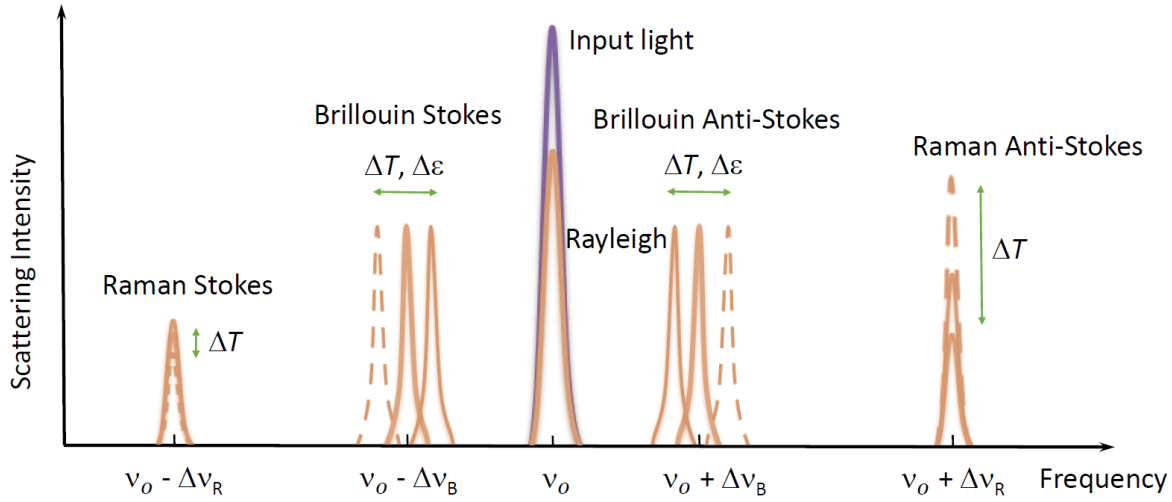


**Figure 11.** A schematic of a spontaneous light scattering spectrum. The sensitivity to temperature changes,  $\Delta T$ , and applied stress,  $\Delta \varepsilon$  is indicated.

1 be obtained via an interferometric technique with OFDR instrumentation by applying  
 2 cross-correlation and taking the difference in the frequency shift between the fiber under  
 3 test and the reference fiber placed elsewhere [92, 112]. For the latter technique, Froggatt  
 4 *et al* [92] estimated “the error in the temperature and strain data” to be 3.5 K and 35  $\mu\varepsilon$ ||,  
 5 respectively, with a spatial resolution of 2 cm over a potential range of 70 m. Note that  
 6 no proper uncertainty budget was provided for this estimate (see also our discussion of  
 7 drawbacks below). Available commercial Rayleigh scattering analyzers focus on detecting  
 8 vibrations and fiber integrity [109].

9 The scattering peaks next to the central Rayleigh peak in figure 11 are called  
 10 Brillouin scattering components and originate from light interactions with propagating  
 11 acoustic phonons in the host material [113]. Brillouin scattering is characterized as  
 12 inelastic scattering: the so called Stokes components are shifted to lower frequencies (the  
 13 photons lost energy in the interaction with acoustic phonons) and the anti-Stokes — to  
 14 higher frequencies (the photons gained energy). The Brillouin frequency shift  $\Delta\nu_B$  can  
 15 be expressed as [108]:

$$16 \quad \Delta\nu_B = \frac{2n_{\text{eff}}V_a}{\lambda_p}$$

17 where  $V_a$  is the velocity of the acoustic wave in the fiber and  $\lambda_p$  is the wavelength of  
 18 the incident light (probe). The Brillouin frequency shift in optical fibers vanishes in  
 19 the forward direction and it is maximized in the backward direction. The amount of  
 20 Brillouin frequency shift is related to the acoustic velocity and the fiber refractive index,  
 21 which are dependent on both the temperature and strain.

||  $\mu\varepsilon$  is a dimensionless unit commonly used in literature to express ppm level change in fractional length

1 A Brillouin scattering fiber sensor system utilizes either spontaneous scattering (e.g.  
 2 Brillouin Optical Time Domain Reflectometry (BOTDR)) or stimulated scattering (e.g.  
 3 Brillouin Optical Time Domain Analysis (BOTDA)), with the latter showing higher  
 4 scattering cross-sections than the former. Stimulated Brillouin scattering (SBS) in optical  
 5 fibers appears when so called pump light of adequate intensity and small bandwidth  
 6 ( $<2$  GHz) at frequency  $\nu_1$  is introduced at one end of the fiber. Simultaneously, a  
 7 counter-propagating probe light at a frequency  $\nu_1 - \Delta\nu_B$  is injected from the other  
 8 end. The input pump pulse generates spontaneous Brillouin scattering at a frequency  
 9  $\nu_1 - \Delta\nu_B$  and the SBS occurs only at the fiber location where the pump and counter-  
 10 propagating probe waves superimpose in time. SBS has better performance in sensing  
 11 length and spatial resolution, as compared to spontaneous Brillouin scattering [114]  
 12 with temperature resolution of 1 K and spatial resolution of 10 m, reported over 22 km  
 13 distance [115]. Note that the temperature resolution above is often wrongly cited as  
 14 the temperature accuracy or measurement uncertainty. Available commercial BOTDR  
 15 and BOTDA analyzers show similar temperature-sensing performance [109]. The key  
 16 drawback of an SBS system is that it needs light, introduced at both ends of the fiber,  
 17 which is not always practical in real-world applications, especially if breakages occur  
 18 during installation e.g. in bridges or roads.

19 Similar to Brillouin scattering, the Raman effect is due to inelastic scattering of light  
 20 where the radiation field exchanges energy with the quantum ro-vibrational energy levels  
 21 of the material [116]. Consequently, Raman scattering also has Stokes and anti-Stokes  
 22 components (see figure 11). The intensities of Stokes and anti-Stokes Raman bands are  
 23 proportional to the the population density of material's ro-vibrational levels which is  
 24 temperature dependent and respond differently to the temperature changes. Thus the  
 25 ratio measurement of Stokes and anti-Stokes Raman bands can be used to determine  
 26 temperature at a distance  $z$  [108]:

$$27 \quad R = \frac{P_{AS}}{P_S} = \left( \frac{\lambda_{AS}}{\lambda_S} \right)^4 e^{(-\alpha_{AS}z + \alpha_S z)} e^{-hc\Delta\nu_R/k_B T}$$

28 where  $\lambda_S$  and  $\alpha_S$  and  $\lambda_{AS}$  and  $\alpha_{AS}$  are the wavelengths and attenuation coefficients  
 29 for Stokes and anti-Stokes light, respectively,  $h$  is the Planck's constant and  $\Delta\nu_R$  is  
 30 the Raman frequency shift. The ratio of the Stokes and anti-Stokes intensities of  
 31 backscattered light can be detected by both OTDR and OFDR techniques. The best  
 32 temperature resolution was reported when the traditional OTDR technique was combined  
 33 with an image de-noising algorithm: 22 mK resolution at 9 km distance with 2 m spatial  
 34 resolution and a short acquisition time of 35 s [117, 118]. Raman-based commercial  
 35 DTSs are currently dominant in distributed photonics sensor technology for temperature  
 36 measurement with sub-kelvin resolution, especially, for long distances [109]. We note that  
 37 fiber-optics have been employed to enable Coherent Anti-Stokes Raman Scattering based  
 38 temperature measurements in harsh environments such as combustion engines [119]. A  
 39 detailed discussion of CARS thermometry and its performance characteristics can be  
 40 found Childs et al's review of established temperature measurement techniques [120].

1 Historically, Raman thermometry has offered relatively poor performance due in part  
2 to low Raman cross-sections, and non-linearity in the detector and spectrometer response.  
3 Using super-conducting nanowire single photon detectors and single photon counting  
4 techniques, spatial resolution of fiber Raman thermometry has been pushed down to  
5 the 1 cm range (limited by spatial modal dispersion) with temperature measurement  
6 uncertainties of 3 K and integration times as little as 60 s [93]. Using the single-photon  
7 detection technique it is theoretically possible to measure thermodynamic temperature  
8 directly through careful characterization of filter bandwidths, filter losses, Raman gain  
9 coefficient, and detection efficiency [93]. The measurement uncertainties though need  
10 to be lowered by several orders of magnitude and the implementation significantly  
11 simplified to make the technique competitive with other primary techniques such as the  
12 near-commercial JNT discussed above.

13 Distributed fiber optic sensors have a unique advantage over traditional point-like  
14 sensors as an equivalent of thousands of sensing points are available for independent  
15 mapping of temperature, strain, vibration, and etc. in three dimensions. On the other  
16 hand, the very same distributed nature of the sensor represents the major challenge  
17 as the current calibration laboratory infrastructure and definition of uncertainty itself  
18 are currently tailored towards point-like sensors instead. Despite some actions by  
19 the DTS community at the international level (i.e. IEC and ASTM standardization  
20 committees [121], US Seafom platform [122]), the dissemination of the DTS technologies  
21 to the involved industries is suffering from a lack of well-established standardization and  
22 rigorous metrological assessment. As a result, DTS literature often relies on figures of  
23 merit such as resolution [123] to communicate measurement confidence. Determination  
24 of detailed uncertainty budget awaits enterprising metrologists [124]. To date, we were  
25 able to find only one metrological assessment of a DTS (Raman) by Laboratoire National  
26 de Métrologie et d'Essais (LNE), France [125, 126]. An additional drawback is that the  
27 commercial DTS so far have been confined to a narrow temperature interval around room  
28 temperature [109, 125]. Extending this working range further with low uncertainties will  
29 be a major challenge as is evident from the work on high-temperature FBGs (see section  
30 4.3). Furthermore, the relative complexity and cost of instrumentation (especially in  
31 case of single-photon Raman measurements) is a deterrent to widespread use.

### 32 4.3. Fiber-Bragg-grating thermometry

33 Fiber Bragg gratings were invented in the 1970s and since then have become widely used  
34 in telecommunications to reflect, filter or disperse light [87]. A fiber Bragg grating is  
35 inscribed in the optical fiber with high-intensity infrared femtosecond lasers or ultraviolet  
36 lasers by means of direct writing or through a phase mask, which creates periodic  
37 variations of the refractive index in the fiber core [87, 127, 128]. These periodic variations  
38 with a period  $\Lambda$  create an interference for a specific wavelength of light, known as the  
39 Bragg wavelength  $\lambda_B$ , for which  $2 \cdot n_{\text{eff}} \cdot \Lambda = \lambda_B$ , where  $n_{\text{eff}}$  is the effective refractive index  
40 of the fiber core at  $\lambda_B$ . A band of wavelengths, centered at the Bragg wavelength that

1 satisfies the Bragg condition for the grating is reflected, whereas non-resonant wavelengths  
 2 are transmitted without any loss (see figure 12). A change in the surrounding temperature  
 3 impacts the effective grating period as it modifies period through the linear thermal  
 4 expansion of the optical fiber and its refractive index due to temperature (TOE)

$$5 \quad \frac{\partial \lambda}{\partial T} = 2 \left\{ \Lambda \frac{\partial n_{\text{eff}}}{\partial T} + n_{\text{eff}} \frac{\partial \Lambda}{\partial T} \right\}$$

6 The thermal response is usually modelled as: a) arising due to the TOE only — since  
 7 the TOE of silica is a factor of ten larger than the thermal expansion [96, 129] — and  
 8 b) as linear. Existing literature indicates that FBG has a temperature dependent shift of  
 9 10 pm/K around room temperature [130] while at elevated temperatures (up to 1000 °C  
 10 for silica fiber) the sensitivity is 14 pm/K [131, 132] although for the most accurate  
 11 sensing applications the FBG response should be assumed to be quadratic [13, 133]. The  
 12 temperature range can be further extended by using sapphire fibers [134]. Note that,  
 13 in general, stress, and anything that causes stress, e.g. fiber curvature or absorption  
 14 of water into the fiber coating, will also shift the resonant wavelength of the FBG  
 15 thermometer. Optimizing the packaging of the thermometer to be stress-free or using  
 16 the the coefficient-matrix method (see e.g. [135–137]) to deconvolute the response to  
 17 temperature and stress, e.g. by designing two gratings with different stress sensitivities,  
 18 will help to eliminate/minimize or quantify the cross-sensitivity, respectively.

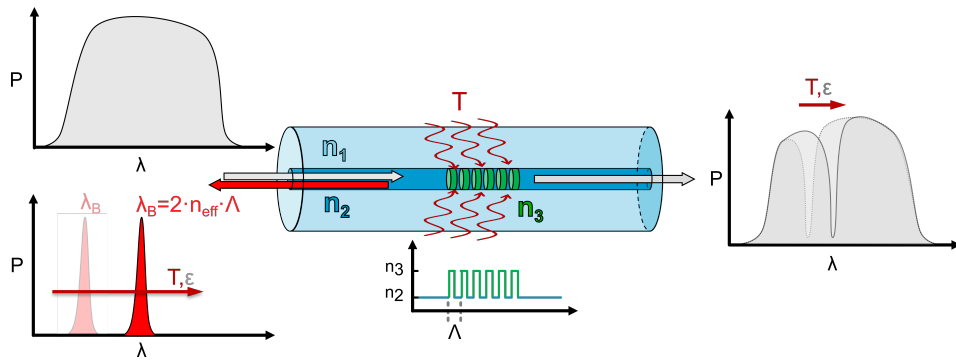


**Figure 12.** Schematic diagram of the transmission and reflection spectra of an optical fiber with an FBG. The FBG results from an index modulation ( $n_3$ ) of spacing  $\Lambda$  inside a single-mode optical fiber.

19 The inherent advantages of fiber-optic sensors that apply to FBG thermometers  
 20 include their compatibility with the existing telecommunications infrastructure, relatively  
 21 low cost and a very small footprint. Typical single mode silica fiber is only 125  $\mu\text{m}$  in  
 22 diameter and the grating length can vary from hundreds  $\mu\text{m}$  to a centimeter. The small  
 23 diameter and cylindrical profile of the fiber mean that the practical FBG thermometer  
 24 can be readily made to resemble the form-factor of a platinum resistance thermometer  
 25 resulting in minimum disruption of the existing infrastructure in many temperature  
 26 measurement applications. In addition, wavelength-encoded measurand information  
 27 enables wavelength-division multiplexing and hence multi-point sensors can be realized  
 28 using this technique.

1        Although FBG thermometers have been widely used for sensing for some time now  
2 and are commercialized, there has been a lack of rigorous metrology driven analysis  
3 of the device performance that is only now beginning to be addressed [13, 17, 21]. For  
4 example, an optimization of strain-free, sealed packaging in order to eliminate FBG's  
5 cross-sensitivity to stress and humidity up to now has not received enough attention. An  
6 examination of Type I grating [87] sensors over a limited temperature range of 233 K to  
7 393 K in dry argon gas environment, in strain-free packaging, indicated that the combined  
8 temperature measurement uncertainty of 0.24 K is dominated by thermal hysteresis  
9 and uncertainty in peak center determination [13]. The latter can be reduced by using  
10  $\pi$ -phase-shifted Type II gratings, since these gratings have a very narrow pass-band  
11 feature in the center of their resonance spectra that results in an average Q-factor of  
12  $10^6$ . However, recent studies [17] of packaged  $\pi$ -phase-shifted Type II gratings in a  
13 closely controlled temperature environment over 273 K – 1273 K temperature range have  
14 confirmed the inherent instability of the gratings, which increases exponentially with  
15 temperature. This conclusion seems to be universal for high-temperature FBGs [33]  
16 and serves to limit the uncertainty performance to a few 100 mK, making FBGs the  
17 photonic equivalent of thermocouples. Available evidence [33, 138, 139] suggests that  
18 thermally driven ion migration between the fiber core and cladding, glass transition  
19 driven stress-strain changes in the fiber and crystallization of  $\alpha$ -quartz phase along  
20 with grating erasure at elevated temperatures can all contribute to the measurement  
21 uncertainty. Understanding the mechanism responsible for the wavelength instability  
22 and quantifying its time-dependent impact on measurement uncertainties is the next  
23 step in the development of FBG thermometers.

#### 24 4.4. Bragg-waveguide grating thermometry

25 An obvious pathway to overcoming the hysteresis in macroscopic FBG sensors is to  
26 develop on-chip gratings where the Bragg grating is written by periodically etching away  
27 small amounts of the waveguide material (see figure 13), effectively creating periodic  
28 regions of low refractive index that collectively act as a grating. This would ensure  
29 that the physical structure of the grating does not change irreversibly with temperature,  
30 while the working principle remains the same as that of an FBG (see section 4.3). Such  
31 devices have been demonstrated to show no discernible hysteresis upon multiple thermal  
32 cycles from 278 K to 433 K [94]. The device also showed excellent repeatability at 293  
33 K when measured repeatedly over a week's time. However, the standard uncertainty  
34 of the device, dominated by the uncertainty in locating the center of the Bragg peak,  
35 was 1.2 K [94]. This uncertainty component is correlated to the peak width which can  
36 be modulated by changing the refractive index contrast ( $\delta_n$ ) between the high and low  
37 index regions of the grating. Accurately tuning the refractive index contrast in SOI  
38 devices can be challenging as it requires precise etching of the waveguide [94, 140, 141].  
39 Furthermore, small, routine fabrication errors translate into significant deviations in  
40 device's effective refractive index, resulting in significant differences between design

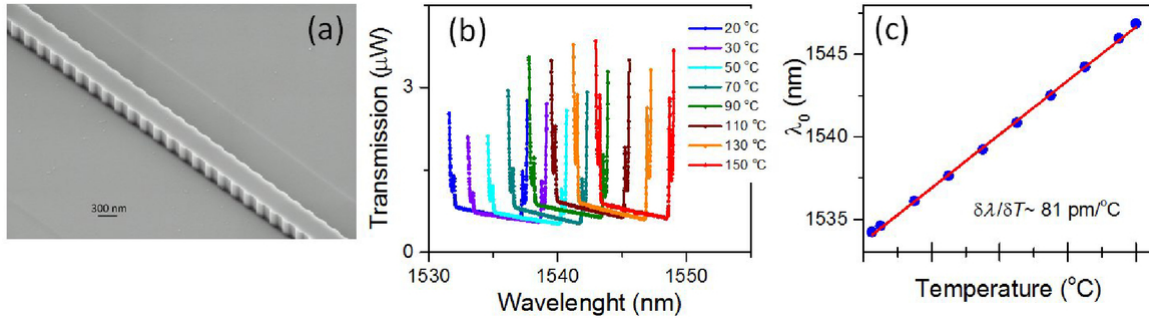


**Figure 13.** Nano-waveguide Bragg grating thermometer: a) SEM image of the part of Si WBG sensor, waveguide cross section is 220 nm × 510 nm, side wall modulation is 60 nm, pitch is 330 nm; b) transmission spectra at different temperatures of SiO<sub>2</sub>-cladded Si WBG thermometer; c) temperature dependence of the center of the stop band (reproduced from [94]).

1 and device resonance wavelength — limiting throughput during production. A more  
 2 cost-effective, more reproducible and easier path to reducing the peak center uncertainty  
 3 is the use of optical resonators, such as ring resonators and photonic crystal cavities.

#### 4 4.5. Ring-resonator thermometry

5 The basic theory of a ring resonator (RR) has been detailed in the literature [142–144]. A  
 6 ring resonator, in its most basic configuration, consists of a closed-loop optical waveguide  
 7 (not necessarily circular in shape) and an adjacent evanescently coupled optical waveguide  
 8 to access the loop, separated by an air gap (see figure 14). The loop supports circulating  
 9 waves that resonate at a wavelength  $\lambda_m$  for which:

$$10 \quad m \cdot \lambda_m = n_{\text{eff}} \cdot L$$

11 where integer  $m$  is the longitudinal resonator mode number,  $n_{\text{eff}}$  is the waveguide effective  
 12 index and  $L$  is the round trip length of the loop. From this relationship it follows that  
 13 the ring resonator spectrum exhibits a periodic notch-filter-like response. As with other  
 14 photonic temperature sensors, the temperature dependence of the ring resonator arises  
 15 from temperature-induced changes in refractive index and the physical dimensions of the  
 16 ring. The temperature-induced shift in wavelength is thus given by [26]:

$$17 \quad \Delta\lambda_m = \left[ \frac{\left( \frac{\partial n_{\text{eff}}}{\partial T} \right) + n_{\text{eff}} \frac{\partial L}{\partial T} \frac{1}{L}}{n_g} \right] (\Delta T * \lambda_m)$$

18 where  $n_g$  is the waveguide group index,

$$19 \quad n_g = n_{\text{eff}} - \lambda_m \frac{\partial n_{\text{eff}}}{\partial \lambda_m}$$

20 The thermal response is usually modelled as: a) arising due to the TOC only — since  
 21 the variation in the refractive index due to the thermal expansion coefficient for silicon  
 22 is a factor of 100 smaller than the silicon TOE [95, 145] — and b) linear. The existing  
 23 literature indicates that a silicon ring resonator has a temperature dependent shift of

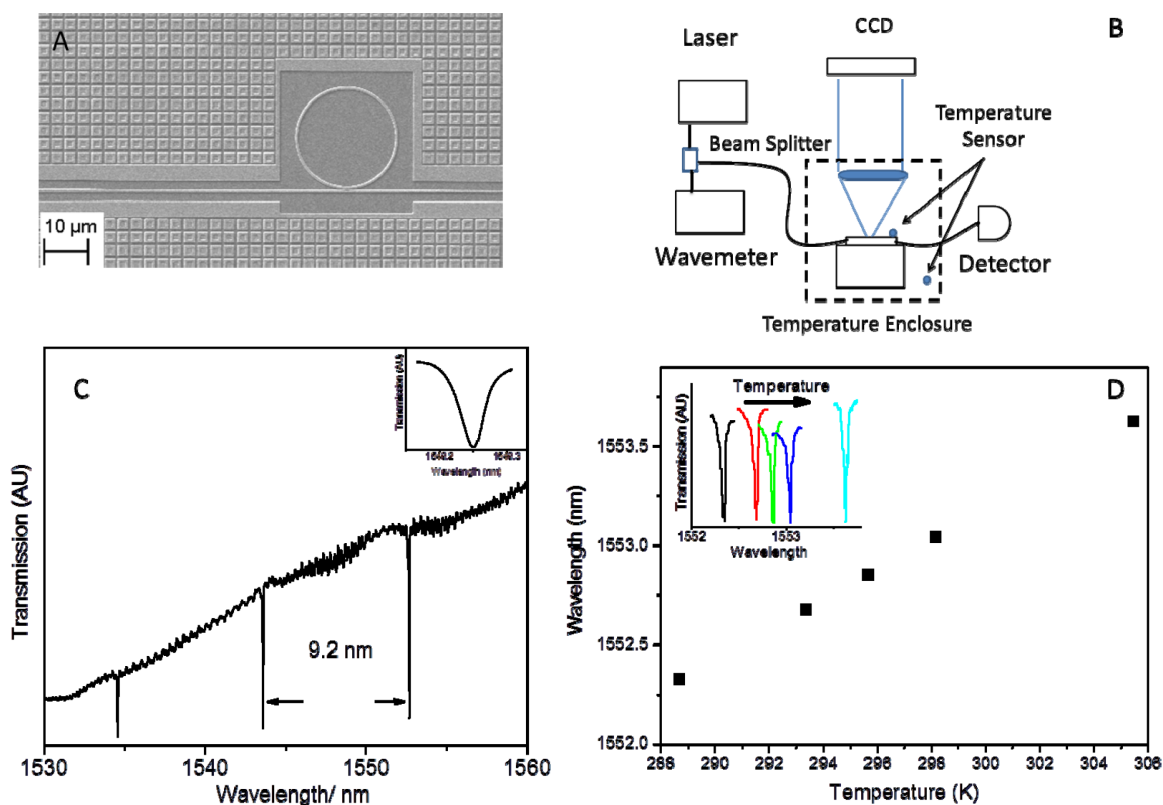


**Figure 14.** a) SEM image of ring resonator device ( $11 \mu\text{m}$  radius,  $130 \text{ nm}$  gap) is shown b) A block diagram of the microscopy-based interrogation set-up used to interrogate the photonic devices is shown. c) The  $11 \mu\text{m}$  radius ring resonator used here shows a free spectral range of  $\approx 9.2 \text{ nm}$  near  $1550 \text{ nm}$ . d) The ring resonator acts as a notch filter whose resonance window is sensitive to temperature changes. The ring's resonance wavelength systematically increases as the temperature increases; resonances at various temperatures are shown in the insert (reproduced from [26]).

1 60–80 pm/K around room temperature [21, 26] although for the most accurate sensing  
 2 applications the RR temperature response should be assumed to be quadratic [146].

3 One of the major advantages of ring-resonator thermometers is the ability to routinely  
 4 fabricate devices with a  $Q$ -factor approaching  $1 \times 10^6$  [24, 25, 147], which allows one to  
 5 significantly reduce the uncertainty in peak-center wavelength measurement (see our  
 6 discussion on resolution in section 2). There exists a wide range of materials, wavelengths  
 7 and device design parameters available for fit-for-purpose device development (see section  
 8 5 for additional discussion).

9 At present routine fabrication imperfections and difficulty in procuring uniform  
 10 thickness wafers limit device interchangeability to 200 mK uncertainty around room  
 11 temperature [148]. At an individual device level, measurements using side-of-fringe  
 12 constant power mode, it has been shown that a noise floor below  $100 \mu\text{K}$  is achieved using  
 13 a free running laser [26]. Using wavelength-swept methods, measurements from cryogenic  
 14 temperatures to above room temperatures have been demonstrated [26, 149]. Packaging

1 of the RR in a practical thermometer was reported to degrade the performance [21],  
 2 however one of the possible reasons in that case was likely a residual porosity of the  
 3 silicon-dioxide cladding layer and, as a result, sensitivity to the humidity. The impact of  
 4 cross-sensitivity with moisture can be largely eliminated by cladding the device with  
 5 densified silica [26, 150]. The other sources of uncertainties include self-heating [22]  
 6 and fabrication imperfections [20]. Effects such as self-heating depend on properties of  
 7 the material (bandgap and heat capacity), operating wavelength, optical quality factor  
 8 of the device itself and input laser power. Using silicon nitride based ring resonators  
 9 and appropriate care in laser power control, the self-heating error can be mitigated to  
 10 below a mK level [151]. Fabrication imperfections can lead to breakdown of symmetry  
 11 between the clockwise and anti-clockwise modes leading to mode splitting and, in rare  
 12 cases, complex line-shape changes that adversely impact measurement uncertainties [20].  
 13 These recent results have highlighted the need to develop documentary standards for  
 14 nanophotonic device fabrication as regards to specific cases in temperature metrology.

#### 15 4.6. Photonic-crystal-cavity thermometry

16 Photonic crystal cavity (PhCC) structures resemble Fabry-Perot like structures much like  
 17  $\pi$ -phase-shifted FBGs. PhCC are created using reactive ion etching (RIE) by utilizing  
 18 two Bragg mirrors fabricated from a periodic array of holes (see figure 15). The mirrors  
 19 are separated by a gap equal to an integer number of the designed wavelength, thus  
 20 forming a wavelength-scale Fabry-Perot cavity with an ultrahigh Q-factor. Due to tight  
 21 confinement of peak electromagnetic field in the cavity, PhCC offer Q-factor to mode  
 22 volume ratios far exceeding that of the ring resonators [152–154], which makes these  
 23 devices ideal for applications in quantum information systems. To avoid scattering losses,  
 24 so called zero-length cavities are designed with a Gaussian distribution of hole sizes  
 25 in a periodic array to confine light [153, 154]. The design parameters can be optimized  
 26 such that the fundamental mode of the cavity appears in the desired wavelength region.  
 27 A practical impact of this design is that it can potentially enable the user to identify  
 28 the mode number of the observed spectral feature without any knowledge of the device  
 29 temperature or modal dispersion [155].

30 Similar to RR PhCC can also have high Q-factors approaching  $1 \times 10^6$  [152, 153].  
 31 As noted above, fabricating high Q-factor devices allows one to reduce the measurement  
 32 uncertainty due to peak center measurement (a limitation in FBG and silicon Bragg  
 33 devices, described above). Klimov *et al*'s results [19] indicate that packaged PhCC  
 34 thermometers enable measurements of temperature with standard uncertainty of 175 mK,  
 35 a  $\approx$  4-fold improvement over the silicon Bragg waveguide thermometer (see section 4.4).  
 36 The uncertainty was dominated by the long-term stability of the thermometer and is  
 37 likely due to residual strain imparted by the epoxy used in the packaging. The impact  
 38 of packaging can be improved by utilizing long waveguides to place the active elements  
 39 away from the bonding region [20].

40 A potential drawback of PhCC design is a slightly lower range of temperature

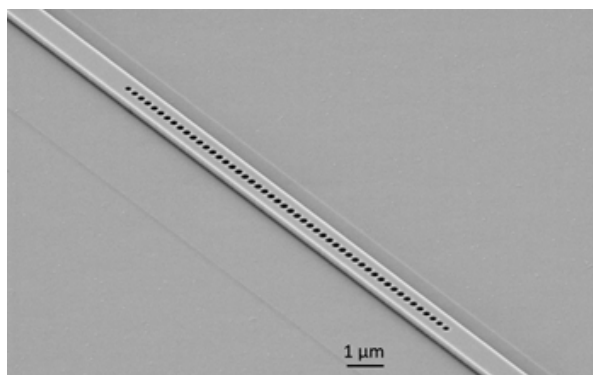


**Figure 15.** SEM image of a silicon nanobeam photonic crystal cavity device (reproduced from [19]).

1 sensitivities (60 pm/K – 70 pm/K) as compared to ring resonators (60 pm/K – 80 pm/K).  
2 Lower temperature sensitivity is due to removal of waveguide material for fabrication  
3 of the low-index holes. The effective refractive index represents a weighted-average of  
4 high-index waveguide material and low-index cladding material (air or SiO<sub>2</sub>), sampled  
5 by the propagating wave. However, we note that the slight reduction in temperature  
6 sensitivity does not appear to limit measurement capabilities, as these devices have been  
7 recently shown to measure temperature at the triple point of water with noise floor  
8 approaching 10 μK [156]. Systematic evaluation of the overall uncertainty in temperature  
9 measurement using such devices, remains an active area of research.

## 10 5. Summary/Outlook

### 11 5.1. Paradigm shift in thermometry

12 The world of temperature metrology is arguably undergoing its most significant disruption  
13 since the advent of the resistance thermometer. The realization of photonic temperature  
14 sensors will eventually move some, possibly even a significant portion, of thermometry  
15 away from electrical based thermometry methods, along with their attendant limitations,  
16 and into frequency measurement domain, opening up an entirely new landscape of  
17 possibilities where photonic temperature sensors can be built with self-diagnosing and  
18 self-adjustment capabilities [74, 155]. In addition, changing the traceability chain could  
19 potentially help in identifying any systematic effects present in the measurements  
20 traceable to electrical units if the two, for some reason, don't agree. It will, however,  
21 require change in training for thermometrists all around the world, to include optics as  
22 they become accustomed to fiber optics, laser locking, Allan deviation and, maybe, even  
23 dual frequency comb spectroscopy. On the other hand, the re-definition of the SI and  
24 the work leading up to it (see introduction to section 3) triggered the development of  
25 field-deployable primary thermometers, covering the entire temperature range from a  
26 few μK to 3000 K. With these new tools, the thermodynamic temperature could soon  
27 be measured directly in industrial settings.

1 In addition, sensor networks — where multiple variables are monitored at the same  
2 time and used to control complex industrial processes in real time — and distributed  
3 sensors — where the sensing information is obtained from hundreds of kilometers  
4 of fiber with a cm spatial resolution over few seconds — together will challenge the  
5 existing temperature calibration infrastructure, and will force us to revisit the important  
6 metrological terms [125], such as uncertainty, traceability and calibration.

7 In the short term, we anticipate that fiber-optic temperature sensors will increasingly  
8 be used in niche applications, e.g. in embedded sensor applications for infrastructure  
9 and in large-area network applications. It is likely that these versatile devices will  
10 continue to find new application areas, e.g. FBG thermometers have been used as  
11 temperature sensing elements in realization of a photonic pH sensor, based on the principle  
12 of photothermal spectroscopy [157] and optomechanical sensors are being developed  
13 for physical and thermodynamic sensing applications, including gravity and force in  
14 addition to temperature measurements [158–160]. High-accuracy primary thermometry  
15 realizations below the silver freezing point (1234.93 K) will likely remain confined to the  
16 national metrology institutes due to the complexity and cost of their implementation,  
17 while lower-accuracy commercial primary thermometers will eventually make their way  
18 to the market.

19 In the long-term, on-chip photonic thermometry could start to compete and possibly  
20 replace SPRTs in calibration facilities. Further developments and deployment of primary  
21 thermometry techniques, such as JNT and on-chip DBT have the potential to provide  
22 zero-chain traceability¶ outside of NMIs. We anticipate that adoption of photonics-based  
23 techniques will create a broad base of users and innovators whose infrastructure build-up  
24 will have an add-on effect: as the cost of exploring new quantum or photonics based  
25 techniques drops, we could witness a marked acceleration of techniques, such as Nitrogen  
26 Vacancy-diamond (NV-diamond) thermometry [161], that currently exists on the outer  
27 fringes of the thermometry horizon.

## 28 5.2. Move towards primary thermometry

29 As described above, the re-definition of the kelvin will promote the use of primary  
30 thermometry [42, 66]. However, it should be acknowledged that at least in the nearest  
31 future such measurements will be confined to cryogenic ( $< 25$  K) and high ( $> 1300$  K)  
32 temperatures, because that is where uncertainties by primary thermometry are already  
33 similar or better than those of the defined scales [66, 162]. In between, the ITS-90 is a  
34 robust low-uncertainty temperature scale, whose values approximate thermodynamic  
35 temperature, so in order to compete, the primary techniques will have to offer other  
36 advantages sought after by the end-users, e.g. the ability to calibrate a thermometer in  
37 situ without physically removing it from the application site as proposed for JNT [8].

¶ Zero-chain traceability refers to the idea of having a top-level temperature realization outside of NMIs. Measurement quality and conformity will still need to be assessed on the regular basis, similar to the current implementation of ITS-90 outside of NMIs.

1 The arrival of field-depolyable JNT is the first step towards deploying a primary  
2 contact thermometer over the temperature range of 25 K and 1300 K. In the past  
3 decade, techniques, such as optical refraction and on-chip DBT have also shown  
4 considerable improvements. Optical refraction, conceived as a primary dimensional  
5 metrology technique and developed as a primary pressure metrology technique, could yet  
6 find itself deployed as a primary thermometer, albeit over a limited temperature range of  
7 100 K to 423 K. Similarly, on-chip DBT is continuing to evolve and could provide access  
8 to primary thermometry in industrial applications with uncertainties of 100 mK or better.  
9 Lastly, opto-mechanical thermometry, an outgrowth of fundamental research in quantum  
10 optomechanics, has shown promise as an on-chip route for realizing thermodynamic  
11 temperature. At cryogenic temperatures it already outperforms traditional stalwarts such  
12 as Coulomb Blockade Thermometry [74]. Recent developments have successfully extended  
13 the measurement range up to 300 K [38] and demonstrated improved measurement  
14 resolution [75]. Further improvements in device design, materials, and measurement  
15 techniques could in the long term improve the measurement uncertainty to the point  
16 of making quantum optomechanics competitive with resistance thermometry, whilst  
17 providing thermodynamic temperature.

### 18 5.3. Future of the defined-scale thermometry

19 Some of the approximations to the defined-scale thermometry techniques, such as  
20 phosphor thermometry (section 4.1), fiber optic thermometry based on Rayleigh, Brillouin  
21 and Raman scattering (section 4.2) and fiber Bragg grating thermometry (section 4.3),  
22 are already commercially available from several vendors. These techniques have found  
23 a foothold in civil infrastructure and industrial applications [83, 86, 109, 163]. For  
24 example, fiber-coupled phosphor thermometry is being used in monitoring nuclear  
25 storage infrastructure [164, 165] while FBGs have been utilized in civil infrastructure such  
26 as bridges and powerplants [83, 86]. Despite their commercial appeal, the metrological  
27 performance of devices such as FBG thermometers is only now being rigorously assessed.  
28 As these devices undergo critical assessment by the metrology community, their potential  
29 roles will be ascertained: recent studies focusing on measurement uncertainty due to  
30 hysteresis suggest that FBG devices are likely to perform as the equivalent of type J  
31 thermocouples, when exposed to temperatures above 353 K [13].

32 On-chip photonic thermometry is potentially a more powerful alternative to both  
33 fiber and resistance thermometry, mainly due to superior properties of constituent  
34 materials (see introduction to section 4). The technique, though still relatively new,  
35 has seen significant developments over the past decade in terms of: materials selection,  
36 design, and fabrication, and performance. Silicon photonic thermometers have been  
37 demonstrated to measure temperature over extensive ranges (4 K to 500 K) with  
38 temperature resolution of as low as 10  $\mu$ K at the triple point of water [156], although, as  
39 recently demonstrated by Zhao *et al* using fiber Fabry-Perot cavities with laser locking,  
40 it is possible to achieve a thermal limit in temperature resolution (160 nK) [166] using

1 photonic sensors. It is anticipated that silicon on-chip photonic thermometers could  
2 cover the range from the triple point of hydrogen (13.8033 K) to the aluminium freezing  
3 point (933.473 K) or higher. Currently the packaging of the devices, such as the bonding  
4 of optical fibers to the chip, limits the temperature range and the long-term stability of  
5 the device [19].

6 While early work with on-chip photonic thermometry focused on silicon-based  
7 devices, the field is rapidly diversifying the choice of materials available, as motivated by  
8 both technical and logistical reasons. Any (future) material to be considered for on-chip  
9 photonic thermometry should at the least:

- 10 (i) Show a low loss at operating wavelengths;
- 11 (ii) Have a suitably high temperature sensitivity (large TOE) and
- 12 (iii) Be thermo-physically stable over a wide temperature range.

13 Based on these requirements, semiconductor-based devices fare better than polymeric or  
14 photoresist based devices as the latter's thermophysical properties limit the application of  
15 the device to temperatures below 500 K. While optical properties of polymeric waveguides  
16 have somewhat improved, at the present they are often two orders of magnitude worse  
17 than semiconductor devices. Furthermore, polymeric waveguides appear to be limited to  
18 the multimode regime which is unsuitable for precision frequency measurements necessary  
19 for achieving 10 mK or better temperature accuracy.

20 The down-selection of semiconductor materials available for photonic thermometry  
21 (Si, SiN, SiC, InP, GaAs, Ge, sapphire and diamond) [167–170] is typically driven by  
22 the choice of operating wavelength and materials used in the photonic foundries. The  
23 wide availability of affordable, tunable, narrow linewidth lasers and detectors at the  
24 telecom C-band 1550 nm wavelength, along with a vast existing infrastructure for silicon  
25 and silicon nitride processing, have made these two materials universally available in  
26 photonic foundries. That said, there are thermometry-specific technical reasons for  
27 exploring different materials, for example, in the past few years, silicon nitride [171] has  
28 gained favour over silicon as the material of choice despite its lower TOE ( $10^{-5}$ ). The  
29 principle advantage of using silicon nitride instead silicon is that the former's bandgap  
30 is located in the UV, as opposed to silicon's (visible). As a result, self-heating due to  
31 two-photon absorption is a less important contributor to the calibration uncertainty for  
32 silicon nitride devices [151] than silicon, where it can rise up to the few percent level  
33 depending upon laser power and device properties [26, 29]. We note that at 1.5  $\mu\text{m}$   
34 range silicon, InP, GaAs provide the highest TOE ( $10^{-4}$  to  $10^{-3}$ ). Introduction of these  
35 materials to foundry processes is in the early stages and could in the future shift the  
36 community's focus away from Si and SiN if the need for ultra-sensitive temperature  
37 measurement arises.

#### 38 *5.4. Instrumentation for emerging technologies*

39 How successful the emerging technologies will be in displacing entrenched legacy  
40 technologies will come down, apart from the performance, to the cost of adopting

1 them, which includes both the financial cost and the cost of changing entrenched industry  
2 standards and practice — the latter often taking a generation. The largest driver of  
3 the financial cost is the device interrogation apparatus, which may include multiple  
4 lasers, wavelength references, photodetectors and related electronics. In general, all the  
5 primary techniques described in section 3 tend to have a very complex and expensive  
6 interrogation apparatus; we therefore anticipate, that in the near future their use will  
7 be confined to NMIs and other specialist research groups. On the other hand, defined-  
8 scale thermometry techniques described in section 4 often avail themselves to size- and  
9 cost-effective solutions.

10 In the latter case, at the minimum, the interrogation set-up will need a narrow  
11 linewidth laser with a sufficiently tuneable wavelength to either track a single resonance  
12 over a wide temperature range [21] or allow coverage of multiple resonances at  
13 any temperature to enable pattern-recognition approach, which uses algorithms to  
14 detect relative changes in two (or more) overlapping resonance patterns with different  
15 temperature sensitivities [172]. In the former case, the tuning range is dictated in part by  
16 material’s TOE and operating temperature range, whilst in the latter it is driven by the  
17 algorithm and device architecture. The cost of the laser and its control electronics can  
18 run from \$3000 for short tuning range ( $\leq 4$  nm) to \$15000 (USD) or more for a widely  
19 tuneable, narrow-linewidth laser suitable for high precision measurement. We note that a  
20 short tuning range lasers such as distributed feedback laser with 4 nm window can cover  
21 temperature spans larger than 4 K for silicon thermometers, or 40 K for silica-based  
22 thermometers.

23 The choice of a wavelength reference similarly depends on the desired uncertainty  
24 budget. For most industrial applications (desired uncertainty of 10 mK to 500 mK), a  
25 gas-wavelength reference with a 0.1 pm wavelength uncertainty, e.g. acetylene ( $C_2^{12}H_2$ ) or  
26 hydrogen cyanide ( $HC^{13}N^{14}$ ), would suffice as a cost-effective measure [23, 173] (a typical  
27 wavelength cell costs \$1000 – \$2000). A 0.01 pm or lower uncertainty will require a more  
28 expensive wavelength meter [26] or a frequency comb [174]. The use of a dual comb  
29 spectrometer can provide near-ideal frequency stability, scan speed and multiplexibility  
30 at the expense of an increase complexity, size and cost. The former will add \$10,000 or  
31 more to the cost on an interrogation set-up, while the latter, depending on bandwidth,  
32 repetition rate, etc. may cost in excess of \$100,000 by itself.

33 Laser-locking techniques [175, 176] can provide improvements in measurement  
34 capability over swept-wavelength schemes that are useful for demanding applications  
35 such as primary calibration laboratories where operators need to achieve uncertainties  
36 on the order of 1 mK to 10 mK. These gains in bandwidth have to be balanced against  
37 increased cost of associated equipment — e.g. a field programmable gated array and  
38 fiber-coupled electro-optic modulator can add an additional \$10,000 to \$30,000 to the  
39 cost of the equipment. Particular use-case driven needs may require the use of additional  
40 artefacts, such as an arrayed waveguide grating or Frizou interferometer, increasing  
41 the cost of wavelength-metrology component from less than a \$1,000 to over \$10,000  
42 with the latter being suitable for high-precision measurements and the former being

1 appropriate for less demanding measurements. On-going work in developing on-chip  
2 frequency standards and construction and validation of cost-effective interrogators for  
3 thermometry applications [23] has the potential to significantly reduce the interrogator  
4 cost and make high-accuracy photonic temperature measurements more affordable. We  
5 anticipate that the parallel evolution of field-deployable primary thermometers and cost-  
6 effective defined-scale photonic thermometers will open up new vistas in temperature  
7 metrology, re-defining the reach of temperature metrology for decades to come.

## 8 Acknowledgments

9 The authors would like to thank Farzana Masouleh, Yije Pan, Dolores Del Campo, Gavin  
10 Sutton and René Eisermann for their constructive contributions to this paper. ZA would  
11 like to thanks this colleague Ryan Fitzgerald, Tobias Herman, Julia Scherschligt and  
12 Amin Tadayon for helpful discussions. SD would like to thank his colleagues, Siegfried  
13 Janz, Dan-Xia Xu, Andrea Peruzzi, Patrick Rourke and Andrew Todd, for carefully  
14 reading the manuscript and providing their feedback. GM acknowledges the support of  
15 the UK government department for Business, Energy and Industrial Strategy through  
16 the UK national quantum technologies programme

## 17 6. References

- 18 [1] Wadhvani P and Yadav S 2020 Temperature sensor market size by product *Global Market Insights*  
19 *Industry Report GMI3469* 1–250
- 20 [2] Nicholas J V and White D R 1994 *Traceable Temperatures (Wiley Series in Measurement Science*  
21 *and Technology)* ed P H Sydenham (Toronto: Wiley) pp 153–198
- 22 [3] Consultative Committee for Thermometry under the auspices of the International Committee  
23 for Weights and Measures 2018 *Guide to the realization of the ITS-90; Platinum Resistance*  
24 *Thermometry* (Paris: BIPM)
- 25 [4] Consultative Committee for Thermometry under the auspices of the International Committee for  
26 Weights and Measures 1997 *Techniques for approximating the international temperature scale*  
27 *of 1990* (Paris: BIPM).
- 28 [5] Mangum B W et al. 2002 Summary of comparison of realizations of the ITS-90 over the range  
29 83.8058 K to 933.473 K: CCT key comparison CCT-K3 *Metrologia* **39** 179–205
- 30 [6] Consultative Committee for Thermometry under the auspices of the International Committee for  
31 Weights and Measures 2019 *Mise en pratique for the definition of the kelvin in the SI* (Paris:  
32 BIPM) <https://www.bipm.org/en/publications/mises-en-pratique>
- 33 [7] Moldover M R, Gavioso R M, Mehl J B, Pitre L, de Podesta M and Zhang J T 2014 Acoustic gas  
34 thermometry *Metrologia*, **51**, R1–19
- 35 [8] Qu J F, Benz S P, Rogalla H, Tew W L, White D R and Zhou K L 2019 Johnson noise thermometry  
36 *Meas. Sci. Technol.* **30** 112001
- 37 [9] Preston-Thomas H 1990 The International Temperature Scale of 1990 (ITS-90) *Metrologia* **27**  
38 3–10
- 39 [10] Preston-Thomas H 1990 The International Temperature Scale of 1990 (ITS-90) *Metrologia* **27** 107  
40 (erratum)
- 41 [11] Foster R J 1986 *Innovation: The Attacker's Advantage* (New York: Summit Books)
- 42 [12] Nicholas J V and White D R 1994 *Traceable Temperatures (Wiley Series in Measurement Science*  
43 *and Technology)* ed P H Sydenham (Toronto: Wiley) pp 114–117

- 1 [13] Ahmed Z, Filla J, Guthrie W and Quintavalle J 2015 Fiber Bragg Grating Based Thermometry  
2 *NCSLI Measure* **10** 28–31
- 3 [14] Laffont G, Cotillard R and Ferdinand P 2013 9000 h-long high temperature annealing of regenerated  
4 Fiber Bragg Gratings *Proc. SPIE, 5th European Workshop on Optical Fibre Sensors* **8794**  
5 87941X
- 6 [15] Laffont G, Cotillard R, Roussel N, Desmarchelier R and Rougeault S 2018 Temperature resistant  
7 fiber Bragg gratings for on-line and structural health monitoring of the next-generation of  
8 nuclear reactors *Sensors* **18** 1791
- 9 [16] Smelser C W, Mihailov S J and Grobnc D 2005 Formation of type I-IR and type II-IR gratings  
10 with an ultrafast IR laser and a phase mask *Opt. Express* **13** 5377–86.
- 11 [17] Dedyulin S, Timakova E, Grobnc D, Hnatovsky C, Todd A D W and Mihailov S J 2021 Accurate  
12 measurements of a wavelength drift in high-temperature silica-fiber Bragg gratings *Metrology* **1**  
13 1–16
- 14 [18] ANSI/ISA S51.1-1979 (R 1993), *Process Instrumentation Terminology*, Instrument Society of  
15 America Standard, December 28, 1979
- 16 [19] Klimov N, Purdy T P, Ahmed Z 2018 Towards replacing resistance thermometry with photonic  
17 thermometry *Sens. Actuators A Phys.* **269** 308–12
- 18 [20] Ahmed Z, Klimov N, Purdy T P, Herman T, Douglass K, Fitzgerald R, Kundagrami R 2019  
19 Photonic thermometry: upending 100 year-old paradigm in temperature metrology *Proceedings*  
20 *Volume 10923, Silicon Photonics XIV* **109230L**
- 21 [21] Dedyulin S, Todd A, Janz S, Xu D-X, Wang S, Vachon M and Weber J 2020 Packaging and  
22 precision testing of fiber-Bragg-grating and silicon ring-resonator thermometers: current status  
23 and challenges *Meas. Sci. Technol.* **31** 074002
- 24 [22] Dickmann W, Weituschat L, Eisermann R, Krenek S, Postigo P A and Kroker S 2021 Heat  
25 dynamics in optical ring resonators *Proc. SPIE, Modelling Aspects in Optical Metrology VIII*  
26 **11783** 1178309
- 27 [23] Eisermann R, Krenek S, Winzer G and Rudtsch S 2021 Photonic contact thermometry using  
28 silicon ring resonators and tuneable laser-based spectroscopy *TM. Tech. Mess.* **88** 640–54
- 29 [24] Xiao S, Khan M H, Shen H and Qi M 2007 Compact silicon microring resonators with ultra-low  
30 propagation loss in the C band *Opt. Express* **15** 14467–75
- 31 [25] Griffith A, Cardenas J, Poitras C B, and Lipson M 2012 High quality factor and high confinement  
32 silicon resonators using etchless process *Opt. Express* **20** 21341–45
- 33 [26] Xu H, Hafezi M, Fan J, Taylor J M, Strouse G F and Ahmed Z J 2014 Ultra-sensitive chip-based  
34 photonic temperature sensor using ring resonator structures *Opt. Express* **22** 3098–104
- 35 [27] Leuthold J, Koos C and Freude W 2010 Nonlinear silicon photonics *Nat. Photonics* **4** 535–44
- 36 [28] Lin Q, Painter O J and Agrawal G P 2007 Nonlinear optical phenomena in silicon waveguides:  
37 Modeling and applications *Opt. Express* **15** 16604–44
- 38 [29] Xu Q F and Lipson M 2006 Carrier-induced optical bistability in silicon ring resonators *Opt. Lett.*  
39 **31** 341–3
- 40 [30] Allan D W 1966 Statistics of Atomic Frequency Standards *Proc. IEEE* **54** 221–30
- 41 [31] Matsko A B, Savchenkov A A, Yu N and Maleki L 2007 Whispering-gallery-mode resonators as  
42 frequency references. I. Fundamental limitations *J. Opt. Soc. Am. B* **24** 1324–35
- 43 [32] Savchenkov A A, Matsko A B, Ilchenko V S, Yu N and Maleki L 2007 Whispering-gallery-mode  
44 resonators as frequency references. II. Stabilization *J. Opt. Soc. Am. B* **24** 2988–97
- 45 [33] Grobnc D, Hnatovsky C, Dedyulin S, Walker R B, Ding H and Mihailov S J 2021 Fiber Bragg  
46 grating wavelength drift in long term high temperature annealing *Sensors* **21** 1454
- 47 [34] Ahmed Z, Cumberland L T, Klimov N N, Pazos I M, Tosh R E and Fitzgerald R 2018 Assessing  
48 radiation hardness of silicon photonic sensors *Sci. Rep.* **8** 13007
- 49 [35] Qu J F, Benz S P, Coakley K J, Rogall H, Tew W L, White R D, Zhou K L and Zhou Z Y 2017 An  
50 improved electronic determination of the Boltzmann constant by Johnson noise thermometry  
51 *Metrologia* **54** 549–58

- [36] Egan P F, Stone J A, Ricker J E, Hendricks J H and Strouse G F 2017 Cell-based refractometer for pascal realization *Opt. Lett.* **42** 2944–47
- [37] Truong G -W, Anstie J D, May E F, Stace T M and Luiten A N 2015 Accurate lineshape spectroscopy and the Boltzmann constant *Nat. Comm.* **6** 8345
- [38] Purdy T P, Grutter K E, Srinnivasan K and Taylor J M 2017 Quantum correlations from a room-temperature optomechanical cavity *Science* **356** 1265–1268
- [39] Rosso L, Tabandeh S, Beltramino G and Fernicola V 2020 Validation of phosphor thermometry for industrial surface temperature measurements *Meas. Sci. Technol.* **31** 034002
- [40] Consultative Committee for Thermometry under the auspices of the International Committee for Weights and Measures 2018 *Guide to the realization of the ITS-90; Triple point of water* (Paris: BIPM)
- [41] Pokhodun A I, Ivanova A G, Duysebayeva K K and Ivanova K P 2015 Final report on COOMET.T-S1. Comparison of type S thermocouples at the freezing points of zinc, aluminium and copper 2014–2015 *Metrologia (Tech. Suppl.)* **52** 03007
- [42] Stock M, Davis R, de Mirandes E and Milton M J T 2019 The revision of the SI — the result of three decades of progress in metrology *Metrologia* **56** 022001
- [43] Stock M, Davis R, de Mirandes E and Milton M J T 2019 Corrigendum: The revision of the SI — the result of three decades of progress in metrology *Metrologia* **56** 049502
- [44] Bureau International des Poids et Mesures (BIPM) 2019 *SI brochure, The International system of units (SI)* 9th Ed (Paris: BIPM) (available at <https://www.bipm.org/>)
- [45] Fischer J *et al* 2018 The Boltzmann project *Metrologia* **55** R1–20
- [46] Gaiser C, Zandt T and Fellmuth B 2015 Dielectric-constant gas thermometry *Metrologia* **52** S217–26
- [47] Gotti R, Lamperti M, Gatti D and Marangoni M 2021 Laser-based primary thermometry: a review *J. Phys. Chem. Ref. Data* **50** 031501
- [48] Newell D B *et al* 2018 The CODATA 2017 values of  $h$ ,  $e$ ,  $k$ , and  $N_A$  for the revision of the SI *Metrologia* **55** L13–16
- [49] Bureau International des Poids et Mesures (BIPM) 2012 *International vocabulary of metrology — Basic and general concepts and associated terms (VIM)* 3rd Ed (Paris: BIPM) (available at <https://www.bipm.org/>)
- [50] Johnson J B 1928 Thermal agitation of electricity in conductors *Phys. Rev.* **32** 97–109
- [51] Brixy H and Kakuta T 1996 *Noise thermometer (JAERI Review 96-003)* (Tokaimura: Japan Atomic Energy Research Institute)
- [52] Nyquist H 1928 Thermal agitation of electric charge in conductors *Phys. Rev.* **32** 110–3
- [53] Callen H B and Welton T A 1951 Irreversibility and generalized noise *Phys. Rev.* **83** 34–40
- [54] Rice S O 1944 Mathematical analysis of random noise part 1 *Bell Syst. Tech. J.* **23** 282–332
- [55] Gati R, Hemmerling B, Folling J, Albiez M and Oberthaler M K 2006 Noise thermometry with two weakly coupled Bose-Einstein condensates *Phys. Rev. Lett.* **96** 130404
- [56] Metrosol 2021 <https://www.johnson-noise-thermometer.com/> (Accessed: 15 October 2021)
- [57] Bramley P, Cruickshank D and Pearce J 2017 The development of a practical, drift-free, Johnson-noise thermometer for industrial applications *Int. J. Thermophys.* **38** 25
- [58] Bramley P, Cruickshank D and Aubrey J 2020 Developments towards an industrial Johnson noise thermometer *Meas. Sci. Technol.* **31** 054003
- [59] Rourke P M C 2021 Perspective on the Refractive Index Gas Metrology Data Landscape *J. Phys. Chem. Ref. Data* **50** 033104
- [60] Egan P, Stone J, Ricker J and Hendricks J 2016 Laser refractometer as a transfer standard of the pascal 2016 *Conference on Precision Electromagnetic Measurements (CPEM 2016)* 1–2
- [61] Ahmed Z, Douglass K O, Eckel S P, Egan, P F, Hendricks J H, Stone Jr J A, 2019 Deformeter for Determining deformation of an optical cavity optic **20200041255A1**
- [62] Ahmed Z, Douglass K O, Eckel S P, Egan, P F, Hendricks J H, Stone Jr J A, 2019 Deformeter for Determining deformation of an optical cavity optic **20200041256A1**

- [63] Ricker J, Douglass K O, Syssoev S, Stone J, Avdiaj S and Hendricks J 2021 Transient heating in fixed length optical cavities for use as temperature and pressure standards *Metrologia* **58** 035003
- [64] Lee J L 2019 FLOC takes flight: first portable prototype of photonic pressure sensor <https://www.nist.gov/news-events/news/2019/02/floc-takes-flight-first-portable-prototype-photonic-pressure-sensor>
- [65] Gianfrani L 2016 Linking the thermodynamic temperature to an optical frequency: recent advances in Doppler broadening thermometry *Phil. Trans. R. Soc. A* **374** 20150047
- [66] Machin G 2018 The kelvin redefined *Meas. Sci. Technol.* **29** 022001
- [67] Machin G, Engert J, Gianfrani L, McEvoy H H and Sparasci F 2018 The European Metrology Programme for Innovation and Research project: Implementing the new kelvin 2 (InK2) *J. Phys.: Conf. Ser.* **1065** 122002
- [68] Castrillo A, Fasci E, Dinesan H, Gravina S, Moretti L and Gianfrani L 2019 Optical Determination of thermodynamic temperatures from a C<sub>2</sub>H<sub>2</sub> line-doublet in the near infrared *Phys. Rev. Applied* **11** 064060
- [69] Truong G -W, Stuart D, Anstie J D, May E F, Stace T M and Luiten A N 2015 Atomic spectroscopy for primary thermometry *Metrologia* **52** S234
- [70] Darquié B, Mejri S, and Sow P L T, Lemarchand C, Triki M, Tokunaga S K, Bordé C J, Chardonnet C and Daussy C 2013 Accurate determination of the Boltzmann constant by Doppler spectroscopy: Towards a new definition of the kelvin *EPJ Web of Conferences* **57** 02005
- [71] Kitching J, Donley E A, Knappe S, Hummon M, Dellis A T, Sherman J, Srinivasan K, Aksyuk V A, Li Q, Westly Q, Roxworthy B and Lal A 2016 NIST on a Chip: Realizing SI units with microfabricated alkali vapour cells *J. Phys.: Conf. Ser.* **723** 012056
- [72] Han Z, Lin P, Singh V, Kimerling L, Hu J, Richardson K, Agarwal A and Tan D T H 2016 On-chip mid-infrared gas detection using chalcogenide glass waveguide *Appl. Phys. Lett.* **108** 141106
- [73] Aspelmeyer M, Kippenberg T J and Marquardt F 2014 Cavity optomechanics *Rev. Mod. Phys.* **86** 1391–1452
- [74] Purdy T P, Yu P-L, Kampel N S, Peterson R W, Cicak K, Simmonds R W and Regal C A 2015 Optomechanical Raman-ratio thermometry *Phys. Rev. A* **92** 031802
- [75] Ferreiro-Vila E, Molina J, Weituschat L M, Gil-Santos E, Postigo P A and Ramos D 2021 Micro-Kelvin resolution at room temperature using nanomechanical thermometry *ACS Omega* **6** 23052–8
- [76] Ren H, Mathoney M H, MacCabe G S, Luo J, Pfeifer H, Mirhosseini M and Painter O 2020 Two-dimensional optomechanical crystal cavity with high quantum cooperativity *Nature Comm.* **11** 3373
- [77] Sudhir V, Schilling R, Fedorov S A, Shultz H, Wilson D J and Kippenberg T J 2017 Quantum correlations of light from a room-temperature mechanical oscillator *Phys. Rev. X* **7** 031055
- [78] Singh R and Purdy T P 2020 Detecting acoustic blackbody radiation with an optomechanical antenna *Phys. Rev. Lett.* **125** 120603
- [79] Chan J, Safavi-Naeini A H, Hill J T, Meenehan S and Painter O 2012 Optimized optomechanical crystal cavity with acoustic radiation shield *Appl. Phys. Lett.* **101** 081115
- [80] Beccari A, Bereyhi M J, Groth R, Fedorov S A, Arabmoheghi A, Engelsen N and Kippenberg T J 2021 *arXiv:2103.09785* [**cond-mat.mes-hall**]
- [81] Ding L, Baker C, Senellart P, Lemaître A, Ducci S, Leo G and Favero I 2010 High frequency GaAs nano-optomechanical disk resonator *Phys. Rev. Lett.* **105** 263903
- [82] Zhang J, Le Roux X, Montesinos-Ballester M, Ortiz O, Marris-Morini, Vivien D L, Lanzillotti-Kimura N D and Alonso-Ramos C 2021 Silicon-on-insulator optomechanical microresonator with tight photon and phonon confinement *arXiv:2103.08465* [**physics.optics**]
- [83] Hecht J 1999 *Understanding fiber optics* (Columbus, Ohio: Prentice Hall) pp 2–38
- [84] Grattan K T V and Meggitt B T (eds) 1998 *Optical Fiber Sensor Technology* vol 2 *Devices and Technology* (London: Chapman & Hall)

- 1 [85] Yu F T S and Yin S (eds) 2002 *Fiber Optic Sensors* (New York: Dekker)
- 2 [86] Rao Y -J 1998 Fiber Bragg grating sensors: principles and applications *Optical Fiber Sensor*  
3 *Technology* vol 2 ed K.T.V. Grattan and B.T. Meggitt (London: Chapman & Hall) pp 355–89
- 4 [87] Othonos A 2000 Bragg gratings in optical fibers: fundamentals and applications *Optical fiber*  
5 *sensor technology* ed K T V Grattan and B T Meggitt (Boston: Kluwer Academic Publishers)  
6 pp 79–187
- 7 [88] Steinvurzel P, Moore E D, Magi E C, Effleton B J 2006 Tuning properties of long period gratings  
8 in photonic bandgap fibers *Opt. Lett.* **31** 2103–5
- 9 [89] Roriz P, Silva S, Frazão O, and Novais S 2020 Optical fiber temperature sensors and their  
10 biomedical applications *Sensors* **20** 2113
- 11 [90] Liu G, Han M and Hou W 2015 High-resolution and fast-response fiber-optic temperature sensor  
12 using silicon Fabry-Pérot cavity *Opt. Express* **23** 7237–7247
- 13 [91] Sumetsky M, Dulashko Y, Fini J M, Hale A and DiGiovanni D J 2006 The microfiber loop  
14 resonator: theory, experiment, and application *J. Light. Technol.* **24** 242–50
- 15 [92] Froggatt M, Gifford D, Kreger S, Wolfe M and Soller B 2006 Distributed strain and temperature  
16 discrimination in unaltered polarization maintaining fiber *Optical Fiber Sensors, OSA Technical*  
17 *Digest (CD)* (Optical Society of America) ThC5
- 18 [93] Dyer S D, Tanner M G, Baek B, Hadfield R H and Nam S W 2012 Analysis of a distributed  
19 fiber-optic temperature sensor using single-photon detectors *Opt. Express* **20** 3456–66
- 20 [94] Klimov N N, Mittal S, Berger M and Ahmed Z 2015 On-chip silicon waveguide Bragg grating  
21 photonic temperature sensor *Opt. Lett.* **40** 3934–6
- 22 [95] Ghosh G 1998 *Handbook of Optical Constants of Solids* ed E D Palik (Toronto: Academic Press)
- 23 [96] Gao H, Jiang Y, Cui Y, Zhang L, Jia J and Jiang L 2018 Investigation on the thermo-optic  
24 coefficient of silica fiber within a wide temperature range *J. Light. Technol.* **36** 5881–86
- 25 [97] Allison S W and Gillies G T 1997 Remote thermometry with thermographic phosphors:  
26 Instrumentation and applications *Rev. Sci. Instrum.* **68** 2615–50
- 27 [98] Brübach J, Pflitsch C, Dreizler A and Atakan B 2013 On surface temperature measurements with  
28 thermographic phosphors: A review *Prog. Energy Combust. Sci.* **39** 37–60
- 29 [99] McSherry M, Fitzpatrick C and Lewis E 2005 Review of luminescent based fibre optic temperature  
30 sensors *Sens. Rev.* **25** 56–62
- 31 [100] Grattan K T V and Zhang Z Y 1998 Fiber optic luminescence thermometry *Optical Fiber Sensor*  
32 *Technology (Optoelectronics, Imaging and Sensing* vol 4) ed K T V Grattan and B T Meggitt  
33 (Dordrecht: Springer)
- 34 [101] Wickersheim K A 1993 Fibre-optic thermometry: an overview *Proc. Int. Conf. Temperature: Its*  
35 *Measurement and Control in Science and Industry* vol 6 ed J F Schooley (New York: AIP Press)  
36 pp 711–4
- 37 [102] Khalid A H and Kontis K 2008 Thermographic phosphors for high temperature measurements:  
38 principles, current state of the art and recent applications *Sensors* **8** 5673–744
- 39 [103] Lowe D, Sutton G, Sposito A, Machin G and Pearce G 2021 Design, construction and traceable  
40 calibration of a phosphor-based fibre-optic thermometer from 0 °C to 650 °C *Meas. Sci. Technol.*  
41 **32** 094004
- 42 [104] Cates M R, Beshears D L, Allison S W and Simmons C M 1997 Phosphor thermometry at  
43 cryogenic temperatures *Rev. Sci. Instrum.* **68** 2412–7
- 44 [105] Cates M, Allison S W, Jaiswal S and Beshears D 2003 YAG:Dy and YAG:Tm phosphorescence to  
45 1700 °C *Proc. of the ISA's 49th Int. Instrumentation Symp* vol 49 pp 389–400
- 46 [106] Hartog A 2000 Distributed fiber-optic sensors: principles and applications *Optical fiber sensor*  
47 *technology* ed K T V Grattan and B T Meggitt (Boston: Springer) pp 241–302
- 48 [107] Bao X and Chen L 2012 Recent progress in distributed fiber optic sensors *Sensors* **12** 8601–39
- 49 [108] Lu P, Lalam N, Badar M, Liu B, Chorpening B T, Buric M P and Ohodnicki P R 2019 Distributed  
50 optical fiber sensing: Review and perspective *Appl. Phys. Rev.* **6** 041302
- 51 [109] Soga K and Luo L 2018 Distributed fiber optics sensors for civil engineering infrastructure sensing

- 1 *J. Struct. Integr. Maint.* **3** 1–21
- 2 [110] Debye P 1947 Molecular-weight determination by light scattering *J. Phys. Chem.* **51** 18–32
- 3 [111] Hartog A H 1983 A distributed temperature sensor based on a liquid core optical fibre *J. Lightwave*  
4 *Technol.* **3** 498–509
- 5 [112] Froggatt M and Moore J 1998 High-spatial-resolution distributed strain measurement in optical  
6 fiber with Rayleigh scatter *Appl. Opt.* **37** 1735–40
- 7 [113] Brillouin L 1922 Diffusion of light and x-rays by a transparent homogeneous body *Ann.Phys.* **9**  
8 88–122
- 9 [114] Bao X and Chen L 2011 Recent progress in Brillouin scattering based fiber sensors *Sensors* **11**  
10 4152–87
- 11 [115] Bao X, Webb D J, Jackson D A 1993 22-km distributed temperature sensor using Brillouin gain  
12 in optical fiber *Opt. Lett.* **18** 552–4
- 13 [116] Long D A 2002 *The Raman Effect: A Unified Treatment of the Theory of Raman Scattering by*  
14 *Molecules* (New York: John Wiley & Sons)
- 15 [117] Soto M, Ramírez J and Thévenaz L 2016 Reaching millikelvin resolution in Raman distributed  
16 temperature sensing using image processing *Proc. SPIE, Sixth European Workshop on Optical*  
17 *Fibre Sensors* vol. 9916 (Limerick, Ireland) 99162A
- 18 [118] Soto M, Ramírez J and Thévenaz L 2016 Intensifying the response of distributed optical fibre  
19 sensors using 2D and 3D image restoration *Nat. Comm.* **7** 1–11
- 20 [119] Hsu R S, Kulatilaka W D, Gord J R and Roy S 2013 Single-shot thermometry using fiber-based  
21 picosecond coherent anti-stokes Raman scattering (CARS) spectroscopy *J. Raman Spectrosc.*  
22 **44** 1330–5
- 23 [120] Childs P R N, Greenwood J R and Long C 2000 A Review of temperature measurement *Rev. Sci*  
24 *Instrum.* **71**, 2959–78
- 25 [121] International Electrotechnical commission 2016 Temperature measurement - Distributed sensing,  
26 IEC 61757-2-2:2016
- 27 [122] Measurement Specifications Working Group 2016 Measurement Specification for Distributed  
28 Temperature Sensing
- 29 [123] Habel W R *et al* 2009 Guidelines for the characterization and use of fibre optic sensors — Basic  
30 definitions & a proposed standard for FBG-based strain sensors *Proc. SPIE, 20th International*  
31 *Conference on Optical Fibre Sensors* vol. 7503 (Edinburgh, United Kingdom) 75035E
- 32 [124] Consultative Committee for Thermometry under the auspices of the International Committee for  
33 Weights and Measures 2021 *Strategy Document for Rolling Programme Development from 2021*  
34 *to 2030* (Paris: BIPM) (available at <https://www.bipm.org/en/committees/cc/cct/publications>)
- 35 [125] Failleau G, Beaumont O, Razouk R, Delepine-Lesoille S, Landolt M, Courthial B, Hénault J  
36 M, Martinot F, Bertrand J and Hay B 2018 A metrological comparison of Raman-distributed  
37 temperature sensors *Measurement* **116** 18–24
- 38 [126] Failleau G, Beaumont O, Delepine-Lesoille S, Plumeri S, Razouk R, Beck Y L, Hénault J  
39 M, Bertrand J and Hay B 2017 Development of facilities and methods for the metrological  
40 characterization of distributed temperature sensing systems based on optical fibres *Meas. Sci.*  
41 *Technol.* **28** 015009
- 42 [127] Mihailov S J 2016 Ultrafast laser inscribed fiber Bragg gratings for sensing applications *Proc.*  
43 *SPIE, Fiber Optic Sensors and Applications XIII* vol. 9852 (Baltimore, Maryland, United  
44 States) 98520P
- 45 [128] Erdogan T 1997 Fiber grating spectra *J. Light. Technol.* **15** 1277–94
- 46 [129] Cavillon M, Dragic P D and Ballato G 2017 Additivity of the coefficient of thermal expansion in  
47 silicate optical fibers *Opt. Lett.* **42** 3650–3
- 48 [130] Mihailov S J 2012 Fiber Bragg grating sensors for harsh environments *Sensors* **12** 1898–918
- 49 [131] Chah K, Yuksel K, Kinet D, Yazd N S, Megret P and Caucheteur C 2019 Fiber Bragg grating  
50 regeneration at 450 °C for improved high temperature sensing *Opt. Lett.* **44** 4036–9
- 51 [132] Celikin M, Barba D, Bastola B, Ruediger A and Rosei F 2016 Development of regenerated fiber

- 1 Bragg grating sensors with long-term stability *Opt. Express* **24** 21897–909
- 2 [133] Flockhart G M H, Maier R R J, Barton J S, MacPherson W N, Jones J D C, Chisholm K E,  
3 Zhang L, Bennion I, Read I and Foote P D 2004 Quadratic behavior of fiber Bragg grating  
4 temperature coefficients *Appl. Optics* **43** 2744–51
- 5 [134] Grobncic D, Mihailov S J, Smelser C W and Ding H 2004 Sapphire fiber Bragg grating sensor  
6 made using femtosecond laser radiation for ultrahigh temperature applications *IEEE Photon.*  
7 *Technol. Lett.* **16** 2505–7
- 8 [135] Guan B-O, Tam H-Y, Tao X-M and Dong X-Y 2000 Simultaneous strain and temperature  
9 measurement using a superstructure fiber Bragg grating *IEEE Photonics Technol. Lett.* **12**  
10 675–77
- 11 [136] Chi H, Tao X M, Yang D X and Chen K S 2001 Simultaneous measurement of axial strain,  
12 temperature, and transverse load by a superstructure fiber grating *Opt. Lett.* **26** 1949–51
- 13 [137] Yu Y, Tam H, Chung W and Demokan M S 2000 Fiber Bragg grating sensor for simultaneous  
14 measurement of displacement and temperature *Opt. Lett.* **25** 1141–3
- 15 [138] Erdogan T, Mizrahi V, Lemaire P J and Monroe D 1994 Decay of ultraviolet-induced fiber Bragg  
16 gratings *J. Appl. Phys.* **76** 73–80
- 17 [139] Baker S R, Rourke H N, Baker V and Goodchild D 1997 Thermal decay of fiber Bragg gratings  
18 written in boron and germanium codoped silica fiber *J. Light. Technol.* **15** 1470–7
- 19 [140] Wang X, Shi W, Yun H, Grist S, Jaeger N A F and Chrostowski L 2012 Narrow-band waveguide  
20 Bragg gratings on SOI wafers with CMOS-compatible fabrication process *Opt. Express* **20**  
21 15547–58
- 22 [141] Wang X, Silicon Photonic Waveguide Bragg Gratings. 2013 PhD Thesis Univ. Br. Columbia
- 23 [142] Van V 2017 *Optical Microring Resonators: Theory, Techniques, and Applications* (Boca Raton,  
24 Florida: Taylor & Francis)
- 25 [143] Bogaerts W, Heyn P D, Vaerenbergh T V, Vos K D, Selvaraja S K, Claes T, Dumon P, Bienstman  
26 P, Thourhout D V and Baets R 2012 Silicon microring resonators *Laser Photonics Rev.* **6** 47–73
- 27 [144] Xu Y, Li Y, Lee R K and Yariv A 2000 Scattering-theory analysis of waveguide-resonator coupling  
28 *Phys. Rev. E* **62** 7389–404
- 29 [145] Lee J - M 2016 Athermal silicon photonics *Silicon Photonics III (Topics in Applied Physics vol*  
30 *122)* ed L D Pavesi and D J Lockwood (Berlin: Springer) 83–98
- 31 [146] Xu D - X, Delège A, Verly P, Janz S, Wang S, Vachon M, Ma P H, Lapointe J, Melati D, Cheben  
32 P and Schmid J H 2019 Empirical model for the temperature dependence of silicon refractive  
33 index from O to C band based on waveguide measurements *Opt. Express* **27** 27229–41
- 34 [147] Gondarenko A, Levy J S and Lipson M 2009 High confinement micron-scale silicon nitride high Q  
35 ring resonator *Opt. Express* **17** 11366–11370
- 36 [148] Klimov N, Berger, M. and Ahmed Z, 2015 Characterization of Ring Resonator Structures for  
37 Applications in Photonic Thermometry, *Advanced Photonics 2015, OSA Technical Digest*  
38 *(online)*, SeT4C.6.
- 39 [149] You M, Lin Z, Li X and Liu J 2020 Chip-scale silicon ring resonators for cryogenic temperature  
40 sensing *J. Light. Technology* **38** 5768–73
- 41 [150] Tao J, Luo Y, Wang L, Cai H, Sun T and Song J 2016 An ultrahigh-accuracy miniature dew  
42 point sensor based on an integrated photonics platform *Sci. Rep.* **6** 29672
- 43 [151] Zhang C, Kang G-G, Wang J, Wan S, Dong C-H, Pan Y-J and Qu J-F 2021 Photonic thermometer  
44 by silicon nitride microring resonator with milli-kelvin self-heating effect *Measurement*  
45 <https://doi.org/10.1016/j.measurement.2021.110494>
- 46 [152] Akahane Y, Asano T, Song B-S and Noda S 2003 High-Q photonic nanocavity in a two-dimensional  
47 photonic crystal *Nature* **425** 944–7
- 48 [153] Deotare P B, McCutcheon M W, Frank I W, Khan M and Loncar M 2009 High quality factor  
49 photonic crystal nanobeam cavities *Appl. Phys. Lett.* **94** 121106
- 50 [154] Quan Q M, Deotare P B and Loncar M 2010 Photonic crystal nanobeam cavity strongly coupled  
51 to the feeding waveguide *Appl. Phys. Lett.* **96** 203102

- 1 [155] Ahmed Z, Photonic resonator analyzer and characterizing a photonic resonator, 2021, US Patent  
2 Application number 17113222
- 3 [156] Klimov N N, Herman T, Douglass K O, Ahmed Z and Chojnacky M J 2021 Ultra-high resolution  
4 nanophotonic thermometry *IMEKO Proceedings* (submitted)
- 5 [157] Hartings M, Castro N J, Gill K and Ahmed Z 2019 A photonic pH sensor based on photothermal  
6 spectroscopy *Sens. Actuators B: Chem.* **301** 127076
- 7 [158] Shomroni I, Qiu L, Malz D, Nunnenkamp A and Kippenberg T J 2019 Optical backaction-evading  
8 measurement of a mechanical oscillator **Nat. Commun.** **10** 2086
- 9 [159] Westphal T, Hepach H, Pfaff J and Aspelmeyer M 2021 Measurement of gravitational coupling  
10 between millimetre-sized masses *Nature* **591** 225–8
- 11 [160] Zhou F, Bao Y, Madugani R, Long D A, Gorman J J and LeBrun T W 2021 Broadband  
12 thermomechanically limited sensing with an optomechanical accelerometer *Optica* **8** 350–6
- 13 [161] Doherty M W, Acosta V M, Jarmola A, Barson M S J, Manson N B, Budker D and Hollenberg L  
14 C L 2000 Temperature shifts of the resonances of the NV-center in diamond *Phys. Rev. B* **90**  
15 041201
- 16 [162] Rourke P M C 2021 ITS-90 reproducibility, xenon fixed point substitution and new interpolating  
17 equations between 13.8033 K and 273.16 K *Metrologia* **58** 055004
- 18 [163] Bao Y, Hoehler M S, Smith C M, Bundy M and Chen G 2020 Measuring three-dimensional  
19 temperature distributions in steel–concrete composite slabs subjected to fire using distributed  
20 fiber optic sensors *Sensors* **20** 5518
- 21 [164] Machin G, Simpson R, Sutton G *et al* 2020 Novel thermometry approaches to facilitate safe and  
22 effective monitoring of nuclear material containers *Nuc. Eng. Des.* **371** 110939
- 23 [165] Sposito A, Heaps E, Sutton G, Machin G, Bernard R and Clarke S 2021 Phosphor thermometry  
24 for nuclear decommissioning and waste storage *Nuc. Eng. Des.* **375** 111091
- 25 [166] Zhao S, Liu Q, Chen J, and He Z 2021 Resonant fiber-optic strain and temperature sensor achieving  
26 thermal-noise-limit resolution *Opt. Express* **29** 1870
- 27 [167] Della Corte F G, Montefusco E M, Moretti L, Rendina I and Cocorullo G 2000 Temperature  
28 dependence analysis of the thermo-optic effect in silicon by single and double oscillator models  
29 *J. Appl. Phys.* **88** 7115–9
- 30 [168] Komma J, Schwarz C, Hofmann G, Heinert D and Nawrodt R 2012 Thermo-optic coefficient of  
31 silicon at 1550 nm and cryogenic temperatures *Appl. Phys. Lett.* 101 041905
- 32 [169] Wemple S H 1973 Refractive-index behavior of amorphous semiconductors and glasses *Phys. Rev.*  
33 *B* **7** 3767–77
- 34 [170] Hu Z G and Hess P 2006 Optical constants and thermo-optic coefficients of nanocrystalline  
35 diamond films at 30–500 °C *Appl. Phys. Lett.* **89** 081906
- 36 [171] Husko C, Ducharme A, Fahrenkopf N M and Guest J R 2021 Phase-shifted Bragg gratings in a  
37 foundry silicon nitride platform *OSA Continuum* **4** 933–9
- 38 [172] Janz S, Cheriton R, Xu D-X, Densmore A, Dedyulin S, Todd A, Schmid J H, Cheben P, Vachon M,  
39 Dezfouli M K and Melati D 2020 Photonic temperature and wavelength metrology by spectral  
40 pattern recognition *Opt. Express* **28** 17409–23
- 41 [173] <https://www.wavelengthreferences.com/products/standard-cells/>
- 42 [174] Gotti R, Puppe T, Mayzlin Y *et al* 2020 Comb-locked frequency-swept synthesizer for high  
43 precision broadband spectroscopy *Sci. Rep.* **10** 2523
- 44 [175] Li G, Ji L, Li G, Su J and Wu C 2021 High-resolution and large-dynamic-range temperature  
45 sensor using fiber Bragg grating Fabry-Pérot cavity *Opt. Express* **29** 18523–29
- 46 [176] Kuroda K 2021 Heterodyne detection applied to a fiber Bragg grating-based sensor using a directly  
47 modulated distributed feedback laser *Opt. Lett.* **46** 3985–8